AD

USAAVLABS TECHNICAL REPORT 70-49A

FATIGUE STRENGTH OF LUGS CONTAINING LINERS

VOLUME 1

RESULTS

By

Robert J. Mayerjak

Paul F. Mahoney

November 1970

U. S. ARMY AVIATION MATERIEL LABORATORIES
FORT EUSTIS, VIRGINIA

CONTRACT DAAJ02-67-C-0066
KAMAN AEROSPACE CORPORATION
BLOOMFIELD, CONNECTICUT

95

DISCLAIMERS

The findings in this report are not to be construed as an official Department of the Army position unless so designated by other authorized documents.

When Government drawings, specifications, or other data are used for any purpose other than in connection with a definitely related Government procurement operation, the United States Government thereby incurs no responsibility nor any obligation whatsoever; and the fact that the Government may have formulated, furnished, or in any way supplied the said drawings, specifications, or other data is not to be regarded by implication or otherwise as in any manner licensing the holder or any other person or corporation, or conveying any rights or permission, to manufacture, use, or sell any patented invention that may in any way be related thereto.

DISPOSITION INSTRUCTIONS

Destroy this report when no longer needed. Do not return it to the originator.

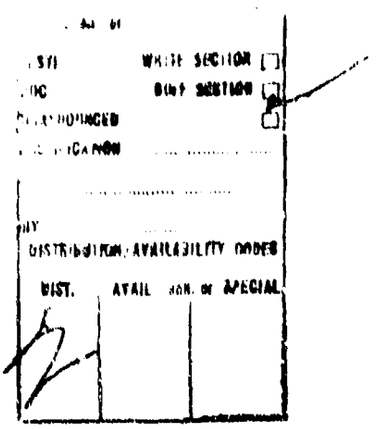

DEPARTMENT OF THE ARMY
HEADQUARTERS U.S. ARMY AVIATION MATERIEL LABORATORIES
FORT EUSTIS, VIRGINIA 23604

The pin-loaded lug is a structural element of considerable importance in aircraft design, particularly in the design of helicopter rotor and control systems. Much work has been done in the analysis of lugs subjected to static loads. As a result, the static analysis of lugs has been reduced to a well-established rational convention, the most notable work being a much-referenced paper by Melcon and Hoblit wherein design allowables and an interaction formula for statically loaded aluminum and steel alloy lugs are reported. In contrast to the static case, no analogous design criterion exists for the design of lugs simultaneously subjected to axial and transverse fatigue loads. A most glaring testimony to the dearth of valid experimental data on pin-loaded lugs is demonstrated in MIL-HDBK-5A, wherein the section on joints offers no design guidance for lugs.

This contract was initiated to:

- Evaluate the fatigue strength of lugs subjected to vibratory loadings at various orientations to the lug axis of symmetry. More specifically, an interaction formula relating load orientation to lug endurance limit was sought.

- Substantiate the photoelastically established benefits in lug fatigue strength that can be derived through selection of interference fit.

- Determine the influence of edge distance and material on lug fatigue strength.

Seventy-three lug specimens were validly tailed by step-testing leading to the development of design charts in the form of modified Goodman diagrams for each material, load direction, and interference fit at two probability-of-failure levels. These charts compare favorably with test results reported in the literature and satisfy structural requirements for a range of edge-distance and load ratios particularly suitable for use in helicopter design. Development of an interaction formula did not materialize. Excessive scatter in the data precluded development of a general interaction formula applicable to both steel and titanium for each edge-distance ratio tested. A specific interaction formula for each configuration tested, although possible, was not pursued.

Results conclusively demonstrate that lug fatigue strength is materially improved by the introduction of high interference fit. Verification of the existence of an optimum interference fit as photoelastically predicted was inconclusive. For the high-modulus materials tested, the level of interference obtainable was limited by attainable thermal size changes. Thus, the "optimum" was the maximum attainable interference fit not causing lug yield. For lugs of lower modulus, such as aluminum or steel and titanium lugs with liners having substantially heavier wall thickness, it is believed that an optimum interference fit does exist beyond which increased interference would be detrimental.

Task 1F162204A14601
Contract DAAJ02-67-C-0066
USAAVLABS Technical Report 70-49A
November 1970

FATIGUE STRENGTH OF LUGS CONTAINING LINERS

Final Report

VOLUME I
RESULTS

Kaman Aerospace Report No. R-850

By

Robert J. Mayerjak
Paul F. Maloney

Prepared by

Kaman Aerospace Corporation
Bloomfield, Connecticut

for

U. S. ARMY AVIATION MATERIEL LABORATORIES
FORT EUSTIS, VIRGINIA

SUMMARY

This report presents the results of an investigation of the fatigue strength of structural lugs. The program included both experimental and analytical phases which were used in a complementary fashion to formulate design charts for fatigue-loaded steel and titanium lugs containing interference fit liners. These lugs are representative of design practice in highly loaded aircraft applications, particularly that found in helicopter blade attaching systems. A primary element in the analytical study was a two-dimensional structural analysis of lug configurations, which was done by finite element methods using a computer program. This computer program is published in Volume II of this report.

The design charts presented will permit the designer to rapidly select lug proportions in either steel or titanium that will satisfy structural requirements for a range of steady and vibratory loading. The designs are considered to be particularly applicable to helicopter rotor and control systems.

FOREWORD

The results of fatigue tests and analyses of lugs are contained in this report. The computer program used for the analyses is presented in detail in Volume II. The project was performed under Contract DAAJ02-67-C-0066, Task 1F162204A14601, and was under the general technical cognizance of Mr. Joseph H. McGarvey of the Aeromechanics Division of USAAVLABS. This contract provided for a unique combination of experimental and analytical efforts to construct design charts for steel and titanium lugs containing liners.

The report consists of two volumes:

Volume I, Results

Volume II, Computer Program Used for Analyses

The tests were conducted in the Structural Test Laboratory of Kaman Aerospace Corporation. The authors wish to acknowledge the contributions of Mr. Hector E. Pelletier, Group Leader, Structural Test, and Mr. Edward R. Luff, Structural Test Engineer, to the successful development of the test rig and to the timely completion of the test program.

TABLE OF CONTENTS

LIST OF ILLUSTRATIONS

LIST OF TABLES

LIST OF SYMBOLS

C_1, C_2 and C_3	parameters for idealized stress-versus-load relationship
d	inside diameter of liner, in.
D	diameter of lug bore, in.
E	Young's modulus of elasticity, ksi
f	internal (or calculated) stress, ksi
f_a	alternating tangential stress in the lug, ksi
f_i	tangential stress in the lug caused by the initial interference fit between the lug and the liner, ksi
f_g	bearing stress (P/DT) that causes the radial stress between the lug and the liner to become zero on the side opposite to the direction of loading, ksi
f_m	mean tangential stress, ksi
F_a	allowable alternating tangential stress, ksi
F_m	allowable mean tangential stress, ksi
H	edge distance for rectangular lug, in.
i	diametral interference between lug and liner, in.
k	one-sided tolernace factor for sample
K_{br}	stress concentration factor for tangential stress from mechanical load. It is the ratio of the maximum tangential stress in the lug at the bore to the average bearing stress, P/DT.
K_i	factor for tangential stress from interference fit. It is the ratio of the tangential stress in the lug at the bore to the tangential stress from the Lamé solution for thick-walled cylinders with diameters d, D, and W, and interference i.

K_r factor for radial stress from mechanical load. It is ratio of the average radial stress over a 90-degree arc of the bore of the lug in a position approximately opposite to the direction of loading to the average bearing stress, P/DT.

K_t stress concentration factor for tangential stress from mechanical load. It is the ratio of the maximum tangential stress in the lug at the bore to the average tensile stress at the net section of the lug, P/T(W-D).

n sample size

p probability of failure

P applied load, kip

R ratio of minimum load to maximum load

R_a load ratio for axial load

R_t load ratio for transverse load

T lug thickness, in.

γ confidence level

θ angular position, deg

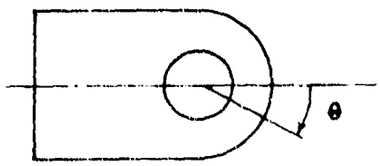

θ_f angular position at which failure occurred, deg

θ_p angular position of load, deg

θ_s angular position of maximum tangential stress, deg

W width of lug, in.

DISCUSSION

Many applications of single-pin structural connections can be found in modern machines and structures. The static strength design of such joints for aircraft has been the subject of a number of studies and has been refined to a considerable degree. Some of the most stringent requirements for connections of this type can be found in helicopter rotor and control systems where high vibratory loads are superimposed on steady loads and the design must have a high level of reliability at minimum weight in this fatigue environment. Large safety factors are not practical. Because of the size and cost of components, it is desirable that they provide long and uninterrupted service installed on the helicopter. The design of major components to meet these goals is approached in a variety of ways in the helicopter industry.

The objective of the present program is to provide background data and analysis leading to the creation of a design criterion for fatigue-loaded lugs. A coordinated experimental and analytical approach to the problem was considered to offer the greatest promise for achieving a practical and successful result. Since it is the long time endurance of lugs that is of most interest, it was decided that a test program which directly evaluated this characteristic, together with a structural analysis that would evaluate the test results in terms of the basic stress levels involved, would be required. To this end a fatigue test program was instituted following the Step Method outlined in reference 1. Test specimens were designed to be representative of the helicopter design practices, and a 1-inch-diameter pin was chosen as a compromise between rotor and control component size. The investigation was treated as a two-dimensional problem since all specimens were loaded in the plane of the lug, which had a uniform 1/2-inch thickness. Pin bending was therefore of constant low order throughout testing. The supporting analysis used a two-dimensional computer program which calculates stresses everywhere in the lug. The computer program, Volume II, uses the matrix displacement method in which the structure (lug) is idealized as an assembly of finite-sized structural elements. From input data which describes these elements and the loading conditions, the computer determines those deflections which will satisfy equilibrium and deflection compatibility at the junctions of the elements. From these deflections, the computer then calculates the stresses in every element. Magnitude and location of failure stresses for all lug configurations were calculated and provided a basis for creation of the lug design criteria.

TEST PROGRAM

SPECIMEN DESIGN

The specimens were machined from 4340 steel heat treated to 175 ksi minimum tensile strength and from titanium alloy, Ti-6AL-4V, annealed, with tensile strength of 130 ksi. These alloys were selected as being representative of many of today's critical lug applications as well as those to be designed in the foreseeable future. This choice also permitted a direct comparison of these two materials, which are often considered to be competitors for a particular component, when used in structural applications. In this case the comparison would be on the basis of material strength in the presence of design and shop practices used in helicopter rotors and would include the deleterious effects of fretting, making the comparison all the more interesting.

As a guide in the choice of lug geometry to be evaluated, a review of some typical lug configurations was conducted. Table I lists the pertinent dimensional data for typical lugs of various sizes. Each represents a critical application, and as such, some level of protection of the lug is provided. A liner or bushing is press-fitted to the lug bore in all cases except those which act as bearing housings, where the bearing outer race provides essentially the same function. The liner acts to protect the lug from inadvertent damage during assembly or disassembly operations, to minimize fretting of the basic lug tension material, and to preload the net lug cross section. The latter two functions are provided through the mechanism of press-fit of the liner. A permanently installed liner can be assembled in the shop with a much higher interference fit than would be practical for pins or other elements that are field-installation items. This high interference induces a roughly uniform radial pressure on the lug-liner interface which apparently inhibits the relative micro-motion between the two parts. This same radial pressure produces a tension load on the net section of the lug. The tension load is always present as a preload of the lug and, therefore, acts to reduce the stress range that results from subsequent applications of external load through the pin.

Interference Fit

The preloading effect resulting from interference fit can best be illustrated by an example. Consider a lug of modest edge distance that has a liner interference fitted to the bore. A load applied to a pin that is closely fitted to the liner is

TABLE I. REPRESENTATIVE FATIGUE-LOADED LUGS USED IN HELICOPTER ROTORS

Component	Lug Material	Lug Width (in.)	Lug Bore Diameter (in.)	W/D	Nominal Diametral Interference (in.)	i/D
Main Rotor						
Hub	Aluminum	6.060	3.000	2.02	.010	.0033
Blade	Aluminum	6.000	2.851	2.10	.016	.0056
Hub	Aluminum	3.500	2.000	1.75	.005	.0025
Retention*	Steel	4.354	3.750	1.16	.0008	.0002
Grip	Steel	4.000	2.256	1.78	.004	.0018
Folding Pin	Steel	3.480	2.250	1.55	.0035	.0016
Tail Rotor						
Grip*	Steel	2.510	2.062	1.22	.0008	.0004
Hub	Steel	2.310	1.750	1.32	.0055	.0031

* Bearing housing

reacted by the lug and causes a variation in stresses throughout the lug. The stress of interest is that associated with the origin of fatigue failure of the lug at the most critical point on the bore. The variation of this stress with applied load is shown in Figure 1. The applied service loading consists of a steady and superimposed vibratory load, as is typical of most helicopter applications. The range of applied load is from P_{min} to P_{max} in Figure 1. The corresponding stress variation for a plain lug that does not have the benefit of preloading would follow the dashed line and would produce a stress range from f_1 to f_2. Introduction of the interference fit liner induces a preload on the net lug section and produces an initial stress, f_i, at the critical point on the lug. Subsequent application of external load through a pin will produce a stress variation following the solid line in Figure 1, and the same load range P_{min} to P_{max} will now produce a stress range from f_3 to f_4. It is clearly seen that the alernating component of stress is substantially reduced by the preloading effect of the liner. There is an

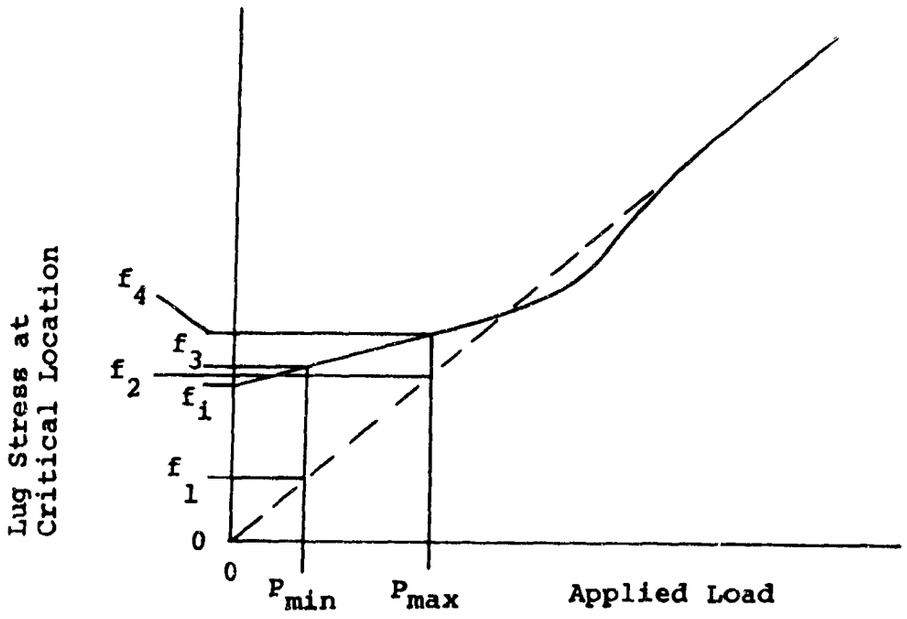

Figure 1. Variation of Critical Lug Stress With Applied Load.

accompanying increase in the mean stress level due to preloading; however, its influence is far less than that of the alternating component. Higher applied loads may, of course, exceed the induced preload, in which case some of the benefit will be lost. This discussion has dealt only with the stresses resulting from interference and applied load but ignores other sources of stress such as machining, heat treating, or cold working which will merely modify the mean stress but leave the general conclusions unchanged. Since the degree of press fit or interference between lug and liner directly affects the preloading and subsequent fatigue performance of the lug, it was considered worthwhile to evaluate the effect of varying interference; this was treated as a parameter in the test program.

The interference fits shown in Table I range from .0002 to .0056 inch per inch of diameter. When components must be assembled in the field, interference fits are usually avoided; however, when assembly is done in a well equipped shop, substantial interference may be obtained with relative ease. Usually the process is assisted by applying heat to the lug to expand it and cooling the liner to shrink its diameter. The temperature differential that is attainable may be limited by the choice of materials and their allowable heat range. When shot-peened parts are involved, care must be taken not to relieve the beneficial residual stresses that are present. For the most critical applications the maximum benefits of interference fit will be sought, while for less critical joints the more easily obtained levels of interference are employed. The highest interference shown in Table I for a steel lug is .0031 inch per inch of diameter. For lugs used in this program with a 1.18-inch bore and using 350°F as the upper limit for lug temperature and -320°F as the liner temperature attainable with liquid nitrogen, it is possible to achieve an interference of approximately .0050 inch. In order that the range of interference investigated would represent practical levels attainable and commonly employed, a low level of .0010 inch was chosen for comparison to a higher level of .0040.

In reference 10, Ligenza suggests the existence of an optimum level of interference beyond which lug fatigue strength would be decreased. The loss in strength is attributed to the high levels of steady stress that occur and the corresponding reduction in allowable vibratory. This type of relation is usually thought of in terms of a Goodman diagram wherein steady stresses approaching the ultimate strength may be accompanied by only low vibratory stresses. In the case of the lug materials used in this investigation, relatively high ultimate strengths are available and the percent of ultimate

achieved with interference-fitted liners is relatively low, on the order of eight percent. It is therefore concluded that lugs of the proportions investigated here will continue to accrue benefits from press fit up to the maximum levels that can be achieved.

Shot-peening

For a further improvement in their fatigue performance, all but one of the lugs listed in Table I are shot-peened. The benefits to be gained from this cold-work operation have been well documented in the literature; the benefits are particularly outstanding in the presence of fretting. Consequently, the incorporation of shot-peening or other cold-work operation for critical joints and fittings has become commonplace in the helicopter industry. It is therefore concluded that a design guide intended for use by helicopter or V/STOL designers should be based on tests of specimens which include shot-peening and press-fit liners.

For these relatively heavy section high-strength lugs, a shot-peen intensity of 12 - 14 A_2 was chosen using SAE 330 shot size. This choice is based largely upon recommended practice and satisfactory experience. In order that coverage of the surface be uniform and complete, one process that has been adopted involves determination of the peening duration which yields 98 percent coverage within a unit area. This duration is then repeated three times for each part that is peened, and the resultant performance of such parts has been found to be excellent.

In an actual service environment, shot-peening serves another very important function. The introduction of a constant high-tensile stress in a critical component by preloading or interference fit has been known to cause or accelerate stress corrosion. This phenomenon, which is a function of the environment and is time dependent, has caused catastrophic structural failures. The existence in close proximity of high-tensile stress levels and corrosive media invites the inception of stress corrosion. Shot-peening produces a surface layer of compressive stress approaching the yield strength of the material, which is of sufficient magnitude to negate the preload induced tensile stresses. Susceptibility of the composite design to stress corrosion is therefore greatly diminished, and many lugs of this design have enjoyed completely successful service use. The influence of interference fit in reducing stress range is still present and fully effective for shot-peened parts.

Width-to-Diameter Ratio

Table I also shows the width-to-diameter ratio, W/D, for the example lugs; the values are seen to range from 1.16 to 2.10. Since the lugs in the table, with one exception, have a circular outer edge concentric with the hole, the lug bore is surrounded by a constant material thickness. Therefore, in cases where it is more convenient to consider lugs in terms of edge distance, the data of Table I can be converted to edge distance ratio by dividing the W/D ratio by a factor of 2.0. The range shown is thought to be typical of critical highly loaded lugs designed for minimum weight. The lowest W/D values are for lugs which form housings for bearings; therefore, they have a larger bore than might otherwise be necessary. To provide specific test data in the area of most interest, values for W/D of 1.30 and 1.69 were chosen as the configurations to be tested. The detailed design of the lug test specimens is shown in Figure 2.

Load Direction

The direction of loading of the structural lugs which form a part of helicopter rotors is often not in line with the axis of symmetry of the lug. Small deviations can be introduced through articulation of the blades; however, much larger angles of load dissymmetry can be found in control system lugs. For example, a typical bellcrank or walking beam clevis will usually be loaded 90° to the axis of symmetry. Other design conditions will be very similar to those for a major rotor component, and much of the above discussion is therefore applicable. To evaluate the influence that load orientation has on lug fatigue strength, it was decided that three specific orientations should be investigated. Those chosen were 0°, 45°, and 90° referred to the lug axis of symmetry.

Load Ratio

Helicopter rotor and control system loadings generally consist of one substantial steady load with superimposed vibratory load. The steady load is derived from centrifugal force either directly as in the blade retention system or in the form of pitching moment reacted by the control system. The vibratory loads, though substantial, will not in the majority of cases exceed the steady load. It is therefore seen that the fatigue cycle for a typical helicopter lug will be a tension-tension type of loading which does not experience load reversal. Accordingly, the load cycle chosen for this study program utilizes a load ratio, R, (P_{min}/P_{max}) of 0.10. This ratio is

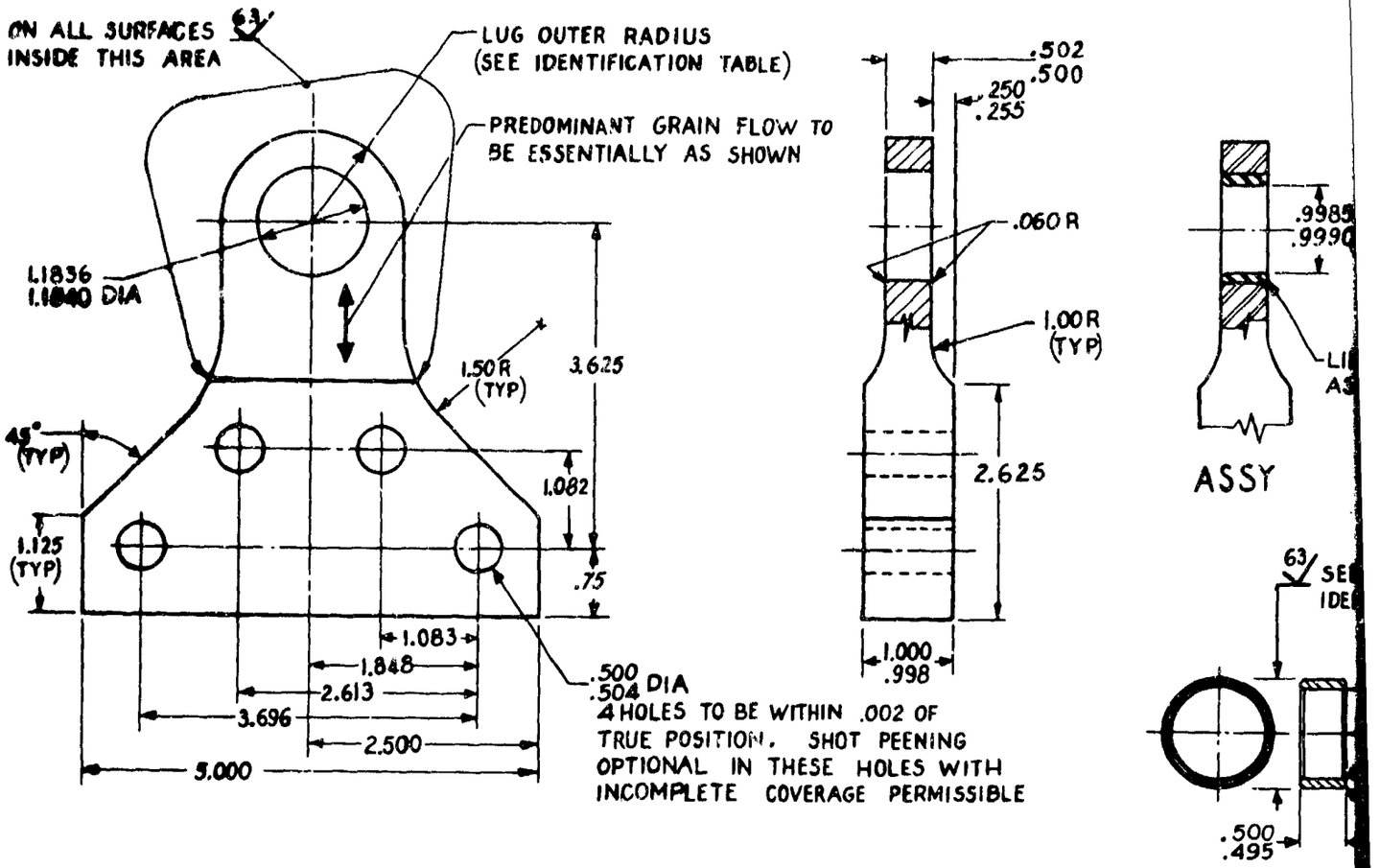

GENERAL NOTES:-

1. MAGNETIC PARTICLE INSPECT OR PENETRANT INSPECT AS APPLICABLE.
2. PARTS TO BE SERIALIZED.
3. SHOT-PEEN LUGS ALL OVER, SHOT SIZE SAE 330, INTENSITY 12-14A2. ALL CORNER RADII TO BE .060 BEFORE PEENING.
4. CADMIUM PLATE LINERS PER SPECIFICATION QQ-P-416 TYPE II, CLASS 3 (.0002-.0003 THK).
5. ASSEMBLE BUSHING & LUG AS FOLLOWS:

   LOWER TEMP OF BUSHING TO -300°F AND RAISE TEMP OF LUG TO +350°F.

   WHEN PARTS HAVE STABILIZED, PRESS BUSHING INTO LUG.

A

LUG SPECIMEN IDENTIFICATION TABLE

IDENTIFICATION NUMBER	LUG MATERIAL	LUG OUTER RADIUS	LINER OUTER DIA AFTER PLATE	ACTUAL INTERFERENCE AFTER SELECTIVE FIT
S_1, S_2, S_3	STEEL	0.767	1.1878	.0038 / .0042
S_4,	STEEL	0.767	1.1848	.0004 / .0010
S_5, S_6	STEEL	1.000	1.1882	.0045 / .0048
S_7	STEEL	1.000	1.1848	.0009 / .0010
T_1, T_2, T_3	TITANIUM	0.767	1.1878	.0039 / .0042
T_4	TITANIUM	0.767	1.1858	.0020 / .0024
T_5, T_6	TITANIUM	1.000	1.1898	.0058 / .0063

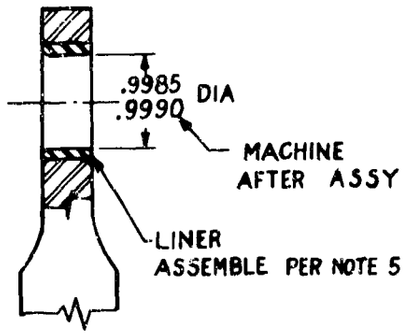

ASSY

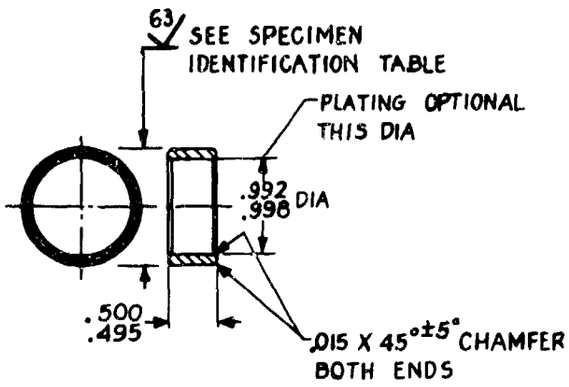

MATERIALS:-

STEEL LUGS 4340 STEEL BAR, MIL-S-5000
HEAT TREATED TO 175 ksi MINIMUM

TITANIUM LUGS Ti-6 AL-4V TITANIUM ALLOY, MIL-T-9047
CLASS 5, ANNEALED

STEEL LINERS 4340 STEEL BAR, MIL-S-5000
HEAT TREATED TO 150 ksi MINIMUM

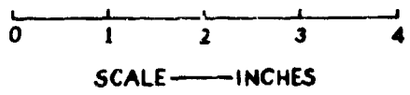

Figure 2. Design of Lug Test Specimen.

considered to be representative of the more critical helicopter lug applications and to give results that will be useful for the design of structural lugs for helicopters. Other load ratios were not investigated in this program.

In summary, the test program was designed to evaluate two materials, two edge distance ratios, three load orientations, and two levels of interference fit. The specific combinations to be tested and the specimen designations are depicted in Table II.

TABLE II. LUG TEST SPECIMEN CONFIGURATIONS

W/D	Interference	Load Direction (deg)			Identification Number	
		0	45	90	Steel	Titanium
1.30	High	X			S1	T1
			X		S2	T2
				X	S3	T3
	Low	X			S4	T4
1.69	High	X			S5	T5
				X	S6	T6
	Low	X			S7	

SPECIMEN FABRICATION

Since the test program was to evaluate the influence of a number of subtle design variations on the fatigue strength of lugs, it was apparent that a number of tests of each configuration would be required. Such replications establish confidence both in the test results and in the controls over the test procedures despite the probable scatter resulting from any fatigue test. Therefore, it was decided that 5 replications for each configuration would be required. Since the test plan called for 13 configurations, 7 steel and 6 titanium, it was apparent that a minimum of 65 specimens must be tested. In reality, 74 specimens were failed in this program by step-testing at increasing vibratory loads until failure.

To preclude the introduction of extraneous variables that might produce erratic results, a number of controls were

instituted for the fabrication of specimens. For each alloy, all material was taken from a single heat of that alloy, all lugs were machined by one vendor as a single production run, all steel lugs were heat-treated as a single batch, all specimens were shot-peened in a single setup, and all bushings were inserted by the same personnel using heat to expand the lugs and liquid nitrogen to reduce bushing size and to ease installation. A final touch-up machining operation was included to rebore the bushing inside diameter and to restore circularity. As an added precaution, a special engineering inspection of bushing outside diameter and lug bore was conducted just prior to assembly. Pairing of bushings and lugs was chosen at that time in such a way as to minimize variations in the resulting press fit for all lugs of a particular configuration. For most configurations the variation in interference was on the order of 0.0002 inch. Slight variations to the above controls were introduced by the need, discovered late in the program, to provide supplemental titanium lugs. These were largely supplied from spare lugs and material from the original lot, and no apparent scatter or deviations were attributed to the supplemental lugs.

A view of finished lug specimens with liners installed is shown in Figure 3.

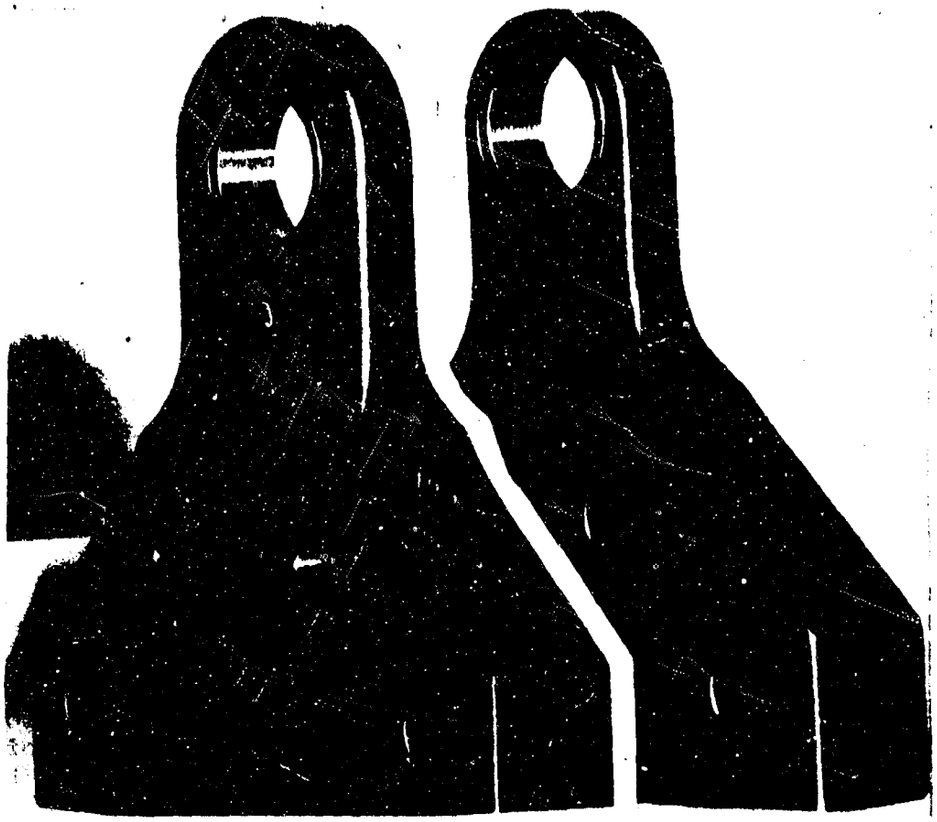

Figure 3. Finished Lug Specimens With Liners Installed.

TEST APPROACH

To put the "design criterion" resulting from this program on as firm a basis as possible, it was desired to generate test results specifically for this purpose. The test specimens were designed to represent the practices most commonly encountered in fatigue-loaded lugs in helicopters. The characteristic of most interest for helicopter application is the fatigue strength of the lug, or the load that the lug will endure for a very large number of cycles. A direct test approach for measuring this characteristic is the "Step Method", wherein each specimen is subjected to a fixed number of cycles at a given vibratory load level before the load is increased to the next level. For the present program and materials, ten million cycles was chosen as the endurance level at which strength was to be evaluated. The size of the load level steps was chosen to approximate five percent of the estimated

lug endurance stress; however, this was influenced by test results and a desire to maintain consistent step magnitudes.

The "Step Method" is sometimes criticized because of the potential influence of "coaxing" on test results. Such an influence has been demonstrated as a strength increase for some alloys but also as a strength reduction for others. The opportunity for a significant strength increase to occur in the presence of fretting during application of low stress amplitudes seems quite remote. More importantly, any long-lived lug in a helicopter structural application will endure many cycles of stress levels below the endurance limit throughout its service life. In fact, it is important to have the fatigue strength of lugs determined in the presence of significant fretting in order that this phenomenon and its deleterious effects will be fully included and accounted for in the final design criterion.

TEST APPARATUS

Since it was the fatigue strength of lugs that was to be evaluated, and the test technique chosen was "step-testing" in ten-million-cycle steps, it was obvious from the outset that a very large number of stress cycles would be accumulated during this program. To accomplish this task expeditiously it was desired that the test rig employed be capable of a high rate of cycle accumulation, with preferably more than one specimen at a time. Peak load levels of approximately 25,000 pounds were anticipated. Review of commercially available equipment revealed that an apparatus capable of meeting these requirements was available but that a substantial capital investment would be required. Also, a single machine of this type would provide a single load path and would not be capable of testing more than two specimens simultaneously.

TEST RIG DESIGN AND ANALYSIS

Study of possible alternatives led to the concept shown schematically in Figure 4. In this arrangement, a central loading cylinder is used to apply a separating force to two beams. Two symmetrically disposed load paths are incorporated with two specimens in each path. A calibrated load link serves to connect the specimens and provide the necessary strain signals for monitoring the test load. Steady loads are introduced to the specimens by pressurizing the load cylinder and developing equal tensile loads in the calibrated links. Vibratory loads are introduced to the specimens by

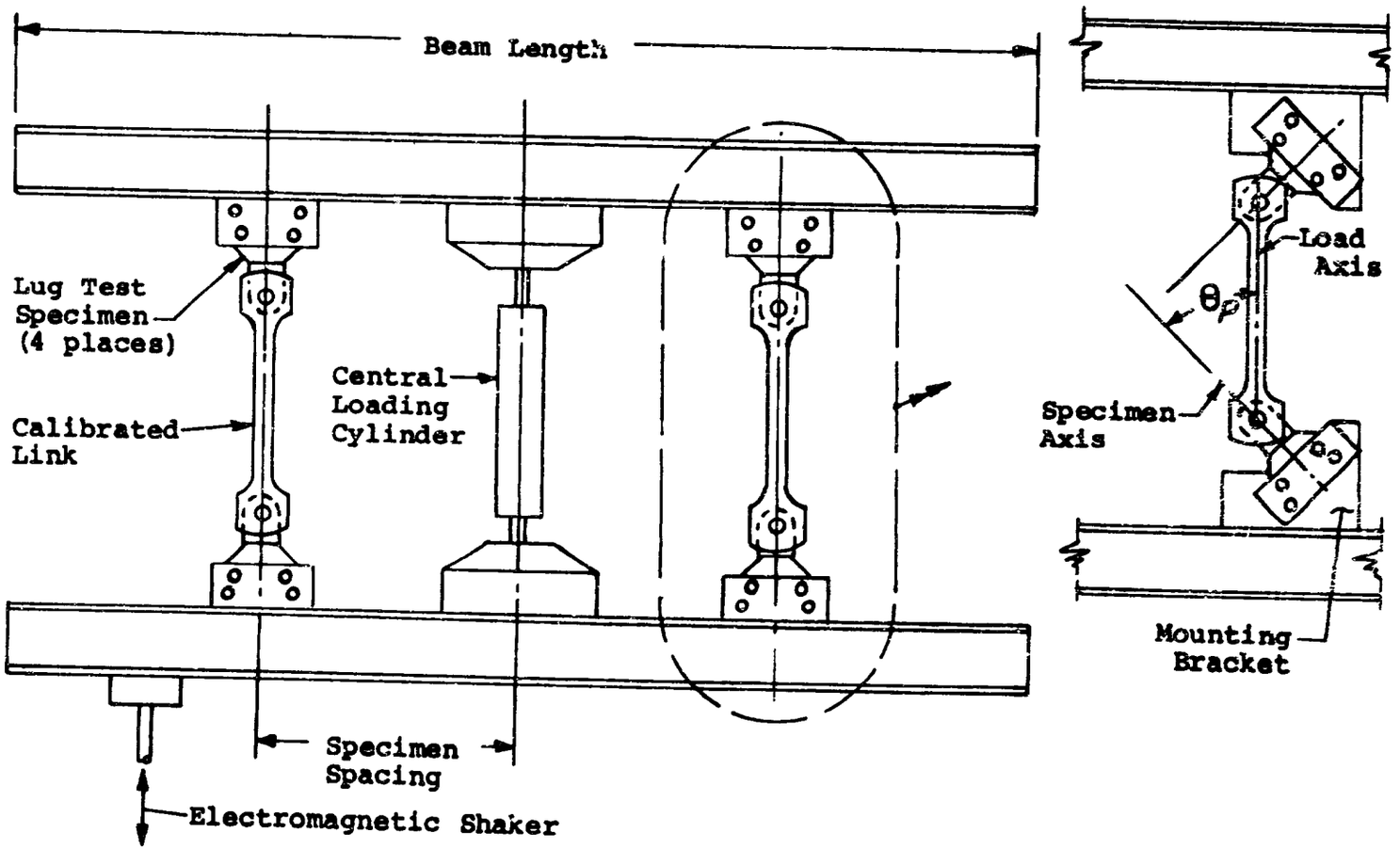

Figure 4. Schematic Representation of Lug Fatigue Test Rig.

exciting this system at one of its natural frequencies and utilizing beam inertia to produce a vibratory load in the calibrated links. Excitation is provided by an electromagnetic shaker and the vibratory load produced is superimposed on the steady load. Controls of steady and vibratory loads are independent, the steady load being controlled simply by cylinder pressure and the vibratory load being controlled by either excitation frequency or power to the exciter. Amplitude of shaker table motion could be kept within acceptable limits by the choice of exciter location along the length of the beam. Loads could be applied to the specimen at any desired angle, θ_p, by use of appropriate mounting brackets to the beam flange as illustrated in Figure 4.

Since the general arrangement seemed to offer many desirable features, a detailed analysis and design of the system was undertaken. To this end a general, contractor developed computer program called General Influence Coefficient (GIC) was utilized to calculate natural frequencies and mode shapes. Beam properties were chosen from those published for standard size commercially available structural shapes. Beam mass and stiffness were well known; however, it was necessary to estimate spring rates for both the specimen load path and for the central loading cylinder. Other variables included in the calculations were beam length, specimen spacing, and the possibility of incorporating beam tip masses. The first two modes of vibration were of interest: one is a symmetric mode in which the tips of a beam move in phase with each other but out of phase with the center; the other mode is asymmetric, with the beam tips moving out of phase and the center acting as a node. These modes are illustrated as follows:

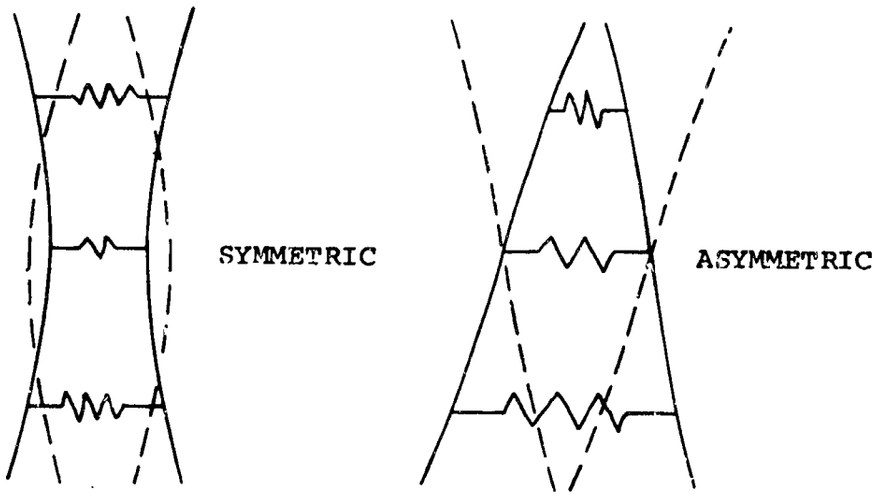

Both modes have the capability of producing adequate specimen loads; however, the asymmetric mode has the additional advantage of not producing vibratory loads in the loading cylinder and, therefore, not introducing an additional source of damping.

Natural frequencies and mode shapes were calculated for 27 parametric variations. The chosen configuration that was designed, built, and used throughout the test program has 12 inch wide flange beams weighing 106 pounds per foot as the main structural members. Beam length was 20 feet, and specimen spacing was 4 feet. With the estimated stiffnesses for specimen path and loading cylinder, the calculated frequencies were 57.9 cps symmetric and 55.7 cps asymmetric. The incorporation of a 200-pound mass at the tips of both beams depressed the frequencies to 42.5 cps and 41.6 cps respectively; however, the potential for achieving higher loads appeared to be improved. Such a reduction in frequency would have a significant effect on test duration and economy; therefore, it was considered that as much testing as possible should be completed without added mass.

RIG DEVELOPMENT

The apparatus described above was set up and operated in a horizontal plane as shown in Figure 5. Each beam was suspended at its mid span to overhead structure, and careful alignment was required in order to eliminate out-of-plane bending of the test lugs. Figure 6 is a general view of the test control station with all primary control and instrumentation apparatus indicated. Figure 7 gives a more detailed view of the specimen and calibrated link installation between the main beams of the rig. Initial trials showed adequate control of loads and frequencies at low values of test load; however, at the higher levels required in the test program, it was not possible to maintain equal vibratory loadings at the two specimen load paths. This was independent of the vibratory mode excited. Varying the position of the electromagnetic shaker changed the load relationship, and it was demonstrated that the central loading cylinder was damping beam vibratory motion so that the specimen path remote from the shaker experienced substantially reduced loads. Use of an all-metal screw jack having vertical line contact to the beam flanges did not significantly alter this characteristic. The final configuration, which proved to be extremely practical, involved the use of a hydraulic cylinder which had its contact with the beam flanges cushioned by a pad of die

Figure 5. General View of Lug Fatigue Test Rig.

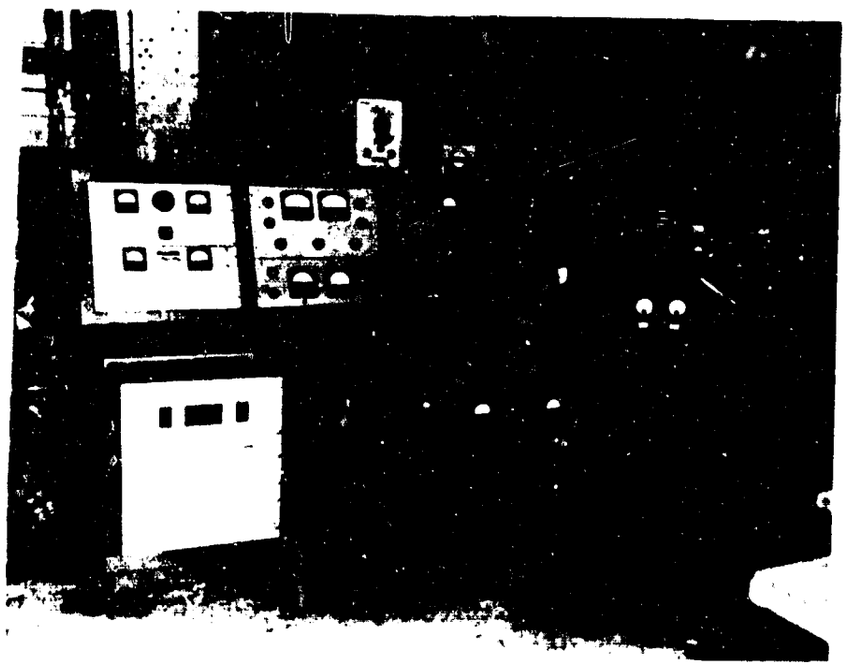

Figure 6. Test Control Station.

rubber 2-1/2 inches thick by 8-1/4 inches in diameter. The durometer of the rubber was approximately 80.

With this configuration it was possible to control loads at both specimen paths by slight frequency adjustments together with changes in exciter power. Final shaker location was 42 inches from one end of a beam. No dissymmetry was introduced in the operation of the test rig by this location despite the apparent dissymmetry due to shaker table mass.

Beam tip masses were evaluated in the development program; however, their use was rejected. The reason for this was that the attachment of a sizable mass in the high "g" field of the beam tips introduced significant damping and therefore was self-defeating. Development of improved connections or integral masses would no doubt overcome this objection; however, it was found to be unnecessary for the present program. The test rig, without added masses, was shown to be capable of producing 18,700 pounds ±15,300 pounds at each specimen position without overloading. Testing was initiated at loading frequencies in the range of 50 cps to 60 cps. The lower frequencies were encountered in testing the 45° and 90° loaded lugs in which the specimen load path had a significantly lower spring rate.

It was recognized that beam misalignment could introduce out-of-plane bending to the lug specimens. This type of loading could introduce a secondary unwanted stress which would tend to confuse test results. Such loadings were readily eliminated by careful alignment of the beams and verification of their absence was provided by the incorporation of a calibrated bending bridge of strain gages on the load link. The output of these gages was constantly monitored however only rare adjustments of beam alignment were required since the setup exhibited little tendency to produce out-of-plane loads.

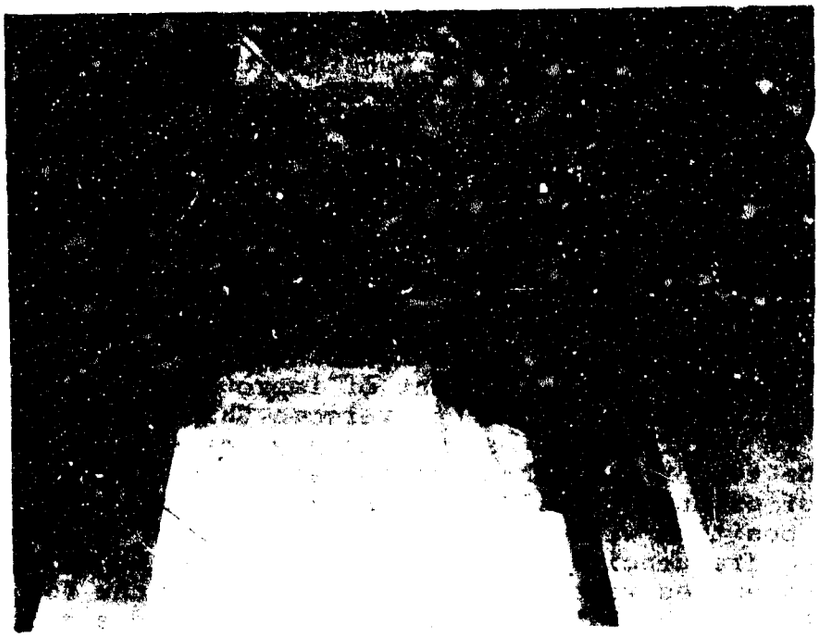

Figure 7. Calibrated Load Link and Specimens.

CONDUCT OF TEST

Once it was firmly established that the test rig operated smoothly at controlled loads, the formal test program was begun. Generally this meant installing four lug specimens of the desired configuration and initiating testing at the preselected steady and vibratory loads. Since all testing was conducted at $R = 0.1$ ($R = P_{min}/P_{max}$), the steady load always exceeded the vibratory load, and the system was essentially preloaded. There was no tendency to oscillate through any clearances that may have existed at the joints. Such clearances were present at the 1-inch-diameter bolts that connected the lugs to the calibrated links. The fit of these bolts to the inside diameter of the bushing in the lug and to the bore of the calibrated link was 0.0000 to 0.0025 inch loose; however, all bushings had been interference fitted to the lugs. As a result, there was more apparent fretting between bolt and bushing than between bushing and lug.

Testing was initiated by introducing the proper steady load to the system through the central loading jack and then vibrating the beams at low amplitudes. The precise resonant frequency of the system was ascertained, and the vibratory load was then increased to the desired level by adjusting frequency and exciter current. Once the running conditions were established, the machine ran virtually unattended, with only periodic monitoring and minor adjustment of loads. This continued until 10^7 cycles had been accumulated at the initial load level. The rig was then shut down, the steady and vibratory loads for the next higher level were established, and steady running was resumed. Successive steps were accomplished in this manner until failure was encountered. Fortunately, failure of a lug was always preceded by a slight drift of rig frequency and loads and final fracture was relatively gentle, consisting of substantial plastic deformation of remaining lug sections. When a lug failed, it was replaced with a dummy having excessive edge distance, and testing was continued. No noticeable change in rig frequency resulted from such substitution.

To apply loads to the specimens in the three desired orientations, three sets of brackets were required. These brackets were bolted to the beams and provided the four-bolt pattern for lug attachment in the proper orientation.

Selecting initial load levels for some configurations presented some difficulty, as evidenced by the number of failures encountered at initial load levels. Alternatively, too low a choice resulted in extended test periods. Experience with the parametric variation being evaluated proved to be the best guide to load-level selection.

One idiosyncrasy that the test rig exhibited was that at the lower load levels encountered, it was difficult to achieve and maintain equal loads at the load links when operating in the asymmetric mode. Operation in the symmetric mode proved to be more stable and dependable at low loads, probably because of the additional damping introduced at the center jack. Tests at the lower loadings were therefore conducted in the symmetric mode.

TEST RESULTS

The fatigue test results are presented in Table III. The table shows the entire number of cycles accumulated on specimens of each identification and serial number. The description of each configuration is presented in Table II. The underlined numbers represent millions of cycles accumulated

TABLE III. FATIGUE TEST RESULTS

Configuration Identification	Serial No.*	Load Level (lb) 2150 ±1770	2900 ±2360	3600 ±2950	4330 ±3540	5050 ±4130	5800 ±4720	6500 ±5310	7210 ±5900	7940 ±6500
S1	1								2.20	
	2								3.30	
	3								10.04	8.45
	4								10.04	0.85
	5						10.00	6.49		
	16					10.00	10.00	7.93		
	21					10.00	10.00	1.27		
S2	11			10.13	10.18	10.10	1.03			
	12			10.13	10.18	10.10	1.51			
	13			10.13	10.18	10.10	4.70			
	14			10.13	10.18	10.10	1.47			
	15					10.10	4.55			
S3	6			10.20	10.18	1.85				
	7			10.20	10.18	0.31				
	8	10.11	10.30	10.18	10.14	10.10	0.96			
	9	10.11	10.30	10.18	10.14	10.10	0.19			
	10	10.11	10.30	10.18	10.14	1.76				
S4	17						2.36			
	18						1.02			
	19						0.67			
	20				1.60					
	22				1.52					
	23				1.21					
	24	10.05	10.01	10.00	6.02					
	25	10.05	10.01	10.00	0.36					
	26		10.12	10.12	2.45					

TABLE III. Continued

Configuration Identification	Serial No. *	Load Level (lb) 2150 ±1770	2900 ±2360	3600 ±2950	4330 ±3540	5050 ±4130	5800 ±4720	6500 ±5310	7210 ±5900	7940 ±6500
T1	1		10.22	10.00	10.00	10.10	0.52			
	2		10.22	10.00	10.00	10.10	10.08	3.04		
	3		10.22	10.00	10.00	10.10	10.08	3.87		
	4		10.22	10.00	10.00	10.10	10.08	1.47		
	5				11.28	10.00	10.00	1.81		
T2	11	9.95	10.13	10.37	0.50					
	12	9.95	10.13	10.37	10.18	1.68				
	13	9.95	10.13	10.37	2.98					
	14	9.95	10.13	10.37	1.30					
	15		10.10	10.12	0.55					
T3	6	10.11	10.30	10.18	1.80					
	7	10.12	10.20	1.21						
	8	10.12	10.20	4.68						
	9	10.12	10.20	5.48						
	10	10.12	10.20	3.17						
T4	11	10.25	10.40	10.09	10.00	1.48				
	12		10.05	10.00	10.00	2.17				
	13		10.05	10.00	10.00	10.08	0.25			
	14		10.00	10.08	10.15	1.38				
	15		10.00	10.08	2.15					

TABLE III. Continued

Configuration Identification	Serial No.*	Load Level (lb) 5800 ±4720	6500 ±5310	7210 ±5900	7300 ±6000	7940 ±6500	8550 ±7000	9800 ±8000	11,000 ±9000	12,250 ±10,000	13,450 ±11,000
	1			7.84		10.99		0.97	← Invalid Origin		
	2			6.74		10.99		11.02	10.07	10.12	1.79
S5	3					10.14		11.02	10.07	10.12	1.47
	4							11.02	10.07	10.12	0.41
	5							10.05	10.07	10.12	1.19
	7							0.82			
	9							0.51			
	10							0.58			
S6	13	10.20			10.12		2.88				
	15	10.20			10.12		2.15				
	18	10.61			10.12		2.45				
	19	10.61			10.12		0.45				
	11	2.71					10.42	0.40			
	12	1.34					1.46				
S7	14						10.42	3.52			
	16						10.42	3.42			
	17		10.00	6.75							
	20		0.82								

TABLE III . Continued

Configuration Identification	Serial No. *	Load Level (lb) 3600 ±2950	4330 ±3540	5050 ±4130	5800 ±4720	6500 ±5310	7210 ±5900	7940 ±6500	9800 ±8000	11,000 ±9000
T5	7						10.12	10.02	7.80	
	8						10.12	10.02	10.10	3.59
	9						10.12	10.02	10.10	1.56
	10						10.12	10.02	10.10	5.12
	11							10.04	2.64	
T6	1	10.02	10.03	10.08	10.18	10.05	5.91			
	2	10.02	10.03	10.08	10.18	10.05	7.73			
	3	10.02	10.03	10.08	10.18	10.05	10.08	5.28		
	4	10.02	10.03	10.08	10.18	10.05	3.49			
	5				10.10	10.50				

* Specimen serial numbers apply to the specific configuration indicated only.

at the failure load level. Failures that have not been preceded by at least one ten-million-cycle runout do not represent an evaluation of the endurance limit of that specimen and hence are not included in the data reduction and evaluation. Approximately two billion load cycles were applied to 74 specimens in the course of the test program. A general view of the failed specimens is shown in Figure 8. Each was metallurgically examined to ascertain the specific fatigue origin location and whether any other factors may have influenced the failure. Only one specimen (configuration S5, serial number 1) failed in an invalid manner, resulting from fretting contact with the clevis of the calibrated load link. All other specimens had valid fatigue origins on the lug bore.

Location of the fracture around the circumference of the bore was strongly influenced by the orientation of the applied load. Figure 9a shows three specimens that were subjected to different load orientations and the accompanying fretting pattern on the lug bore. In each instance the primary fracture appears on the right in the picture. It will be noted that in each case the fracture is associated with an area of heavy fretting. Examination of the complete lug bore revealed that in each case the lug fracture occurred within the area of most severe fretting. Figure 9b illustrates the character of the fracture of specimen S-3, serial number 9 including the location of multiple fatigue origins. Figure 9c shows a typical liner crack and the pattern of fretting that occurred between bolt and liner. Exact angular position of each fracture was carefully determined so that this position could be correlated with calculated stresses. Table IV presents the average location of primary fracture surface for each configuration in terms of the angle θ measured from the lug axis of symmetry. The usual range of observed failure locations for a single test configuration was 15°, with only one configuration having a range of 25°.

The fracture location is seen to have a fairly consistent relation to load orientation. For the axially loaded specimens, rudimentary considerations would anticipate failure at the net section of the lug, the 90° position. Table IV shows that in fact all axially loaded configurations failed at angular locations that exceeded 90° in an area significantly removed from the minimum cross section. Observation of failed specimens showed that the failures were invariably associated with the site of heavy apparent fretting. The fretting pattern on the lug bore of the axially loaded specimens showed essentially no fretting in the center of the applied load zone. At the 90° position, only light fretting was apparent; however, the area of heavy fretting, characterized by much darker

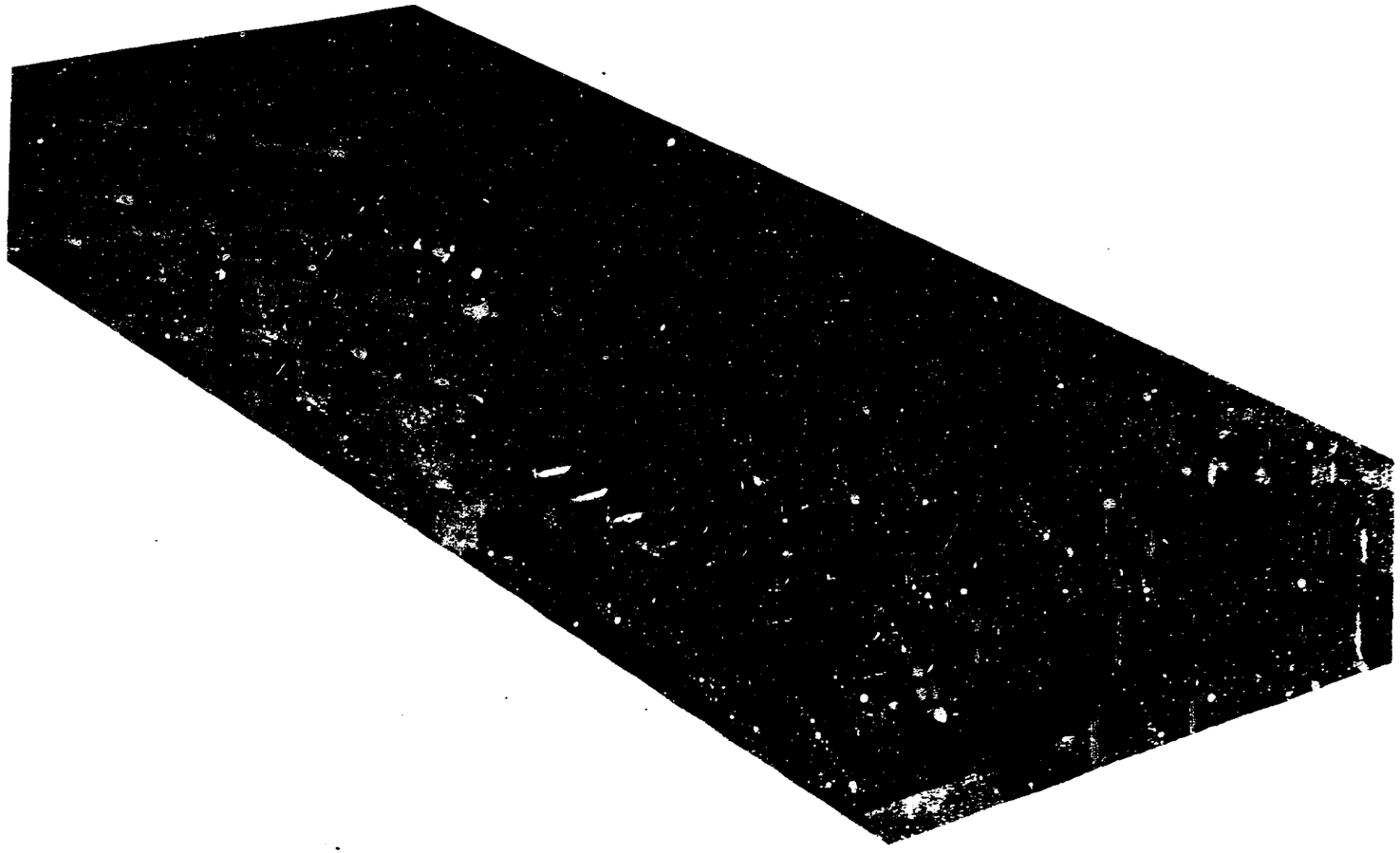

Figure 8. Failed Lug Fatigue Test Specimens

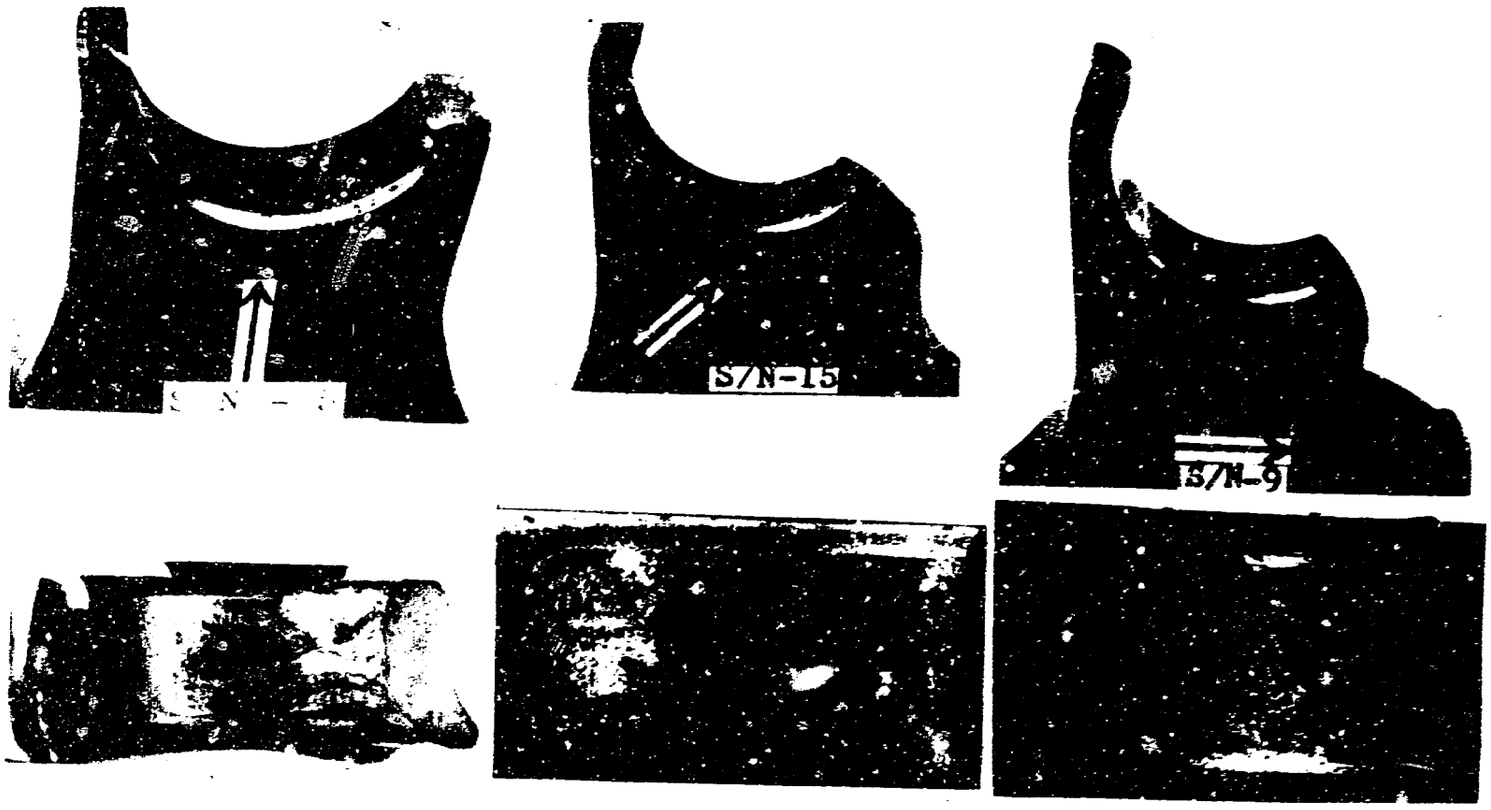

Configuration S1
Serial No. 5

Configuration S2
Serial No. 15

Configuration S3
Serial No. 9

Figure 9a. Specimen Fracture Orientation and Fretting Pattern.

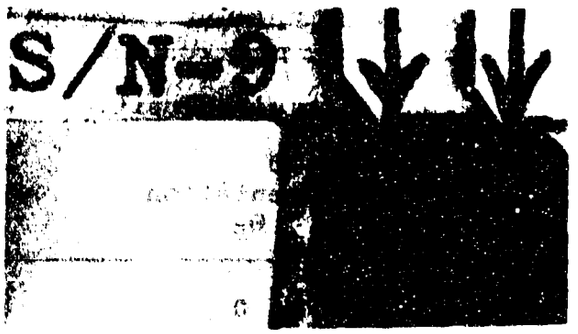

Figure 9b. Closeup of Fracture Surface, Specimen S3, Serial No. 9.

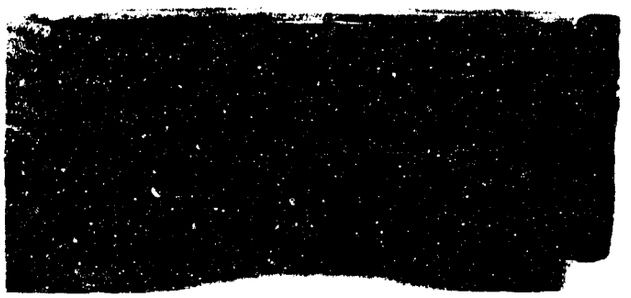

Figure 9c. Typical Liner Crack and Fretting Pattern.

surface and debris deposits, usually began at an angular position just beyond the 90° point. The fatigue origins were within the area of heavy fretting. The edge of the area of heavy fretting was slightly influenced by the level of liner interference, high interference causing the area of heavy fretting to occur at slightly larger values of θ.

TABLE IV. LOCATION OF PRIMARY FRACTURE SURFACE

Configuration	Angular Position (deg)* Load Orientation θ_p	Fracture Orientation θ_{f}**
S1	0	108
S2	45	146
S3	90	157.5
S4	0	102
S5	0	102.5
S6	90	154
S7	0	104
T1	0	105
T2	45	140
T3	90	156
T4	0	109
T5	0	98
T6	90	155

* Measured from lug axis of symmetry.
** Fracture orientations listed are average. Maximum spread from average was $\pm$ 12.5°.

The location of the fatigue origin with respect to the thickness of the lug was also carefully noted. Pin bending could be expected to concentrate load and stress near the edge of the hole at the lug faces. All hole edges had a 0.060-inch radius, and contact with the liner therefore began at the tangency point of this radius with the lug bore. The general location of fatigue origins was 1/16 to 1/8 inch in from this tangency point toward the center of lug thickness. However, a sufficient number of specimens had origins at or very near the center of the specimen to verify the original supposition that pin bending was of low order and not of significance in test results. This same observation provided a further demonstration that the test rig did not introduce bending to the specimen.

Of the 74 specimens failed in fatigue, approximately one-half exhibited cracks in the liners upon posttest examination. These cracks originated at the inside diameter where generally heavy fretting occurred between pin and liner. Most liner cracks penetrated the wall thickness; however, some were limited to only a small portion of the wall and did not reach the liner-lug interface. The potential influence of this phenomenon on lug performance was constantly monitored In general, the liner cracks, which emanated from the site of heavy fretting between pin and liner, occurred at angular orientations of less than 90° for axially loaded specimens, while lug fractures were at locations in excess of 90°. The possibility of a direct influence under these conditions seemed remote. In addition, a special review of test results was conducted for the purpose of revealing whether any influence from liner cracking was apparent. The review showed that the performance of specimens with cracked liners was thoroughly intermixed with that of specimens in which the liners did not crack. No pattern was discernible, and it was therefore concluded that cracks in liners had no apparent influence on lug strength. It must be remembered that all liners in this program were interference fitted to the mating lug and were therefore in a general state of compression. Under these conditions, the opportunity for liner relative motions to cause damage to the lug bore is minimized. The fact that the liners themselves cracked under these conditions is probably attributable to the tangential stresses generated by surface tractions in the heavy fretting area between pin and liner.

The test results presented in Table III are analyzed and correlated to theoretical stress calculations in a subsequent section of this report. These results are then used as a guide in establishing design charts for fatigue-loaded lugs. The preparation of these charts makes use of the ultimate strength of lugs. To calculate the ultimate strength of titanium lugs, it was assumed that the curves presented in reference 2 for steel lugs also applied to titanium lugs. This assumption was found to be consistent with the results, shown below, for two static tests that were made on titanium lugs loaded transversely, $\theta_p = 90^\circ$.

	Ultimate Load, kips		Percent
W/D	Test	Calculated	Error
1.3	26.50	25.01	-5.6
1.69	44.27	46.18	4.3

TEST INTERPRETATION

METHOD FOR CALCULATING FATIGUE STRENGTH

A method was developed for calculating the fatigue strength of lugs subjected to a large number of load repetitions greater than 10^7. The method is based upon simplifying assumptions, idealized models, an idealized stress-versus-load relationship and allowable stresses deduced from correlations of the method with results from fatigue tests of lugs. Each basis is reviewed in the following sections.

Assumptions

There are five principal assumptions:

1. The allowable fatigue strength for a material of given composition, heat treatment, and surface treatment can be defined by a constant-life line on a modified Goodman diagram, which is plotted using only tangential components of elastic stresses in the lug at the bore.

2. Some stresses may be omitted from the detailed calculation of alternating stress and mean stress. These omitted stresses include residual stress resulting from shot-peening, and frictionally induced stress from relative motions between the lug and the liner.

3. The effect of the omitted stresses upon the fatigue strength of the lug can be accounted for by using a constant-life line established from fatigue tests of lugs.

4. The stress versus load relationship does not change during the life of the lug.

5. The stress versus load relationship can be defined by three straight-line segments.

Idealized Models

Figure 10 shows the stress-versus-load relationship for four different types of lugs. The solid-line curve corresponds to a typical real lug containing an interference-fitted liner with a closely fitted pin. The dotted lines correspond to three idealized lugs, each containing a closely fitted liner

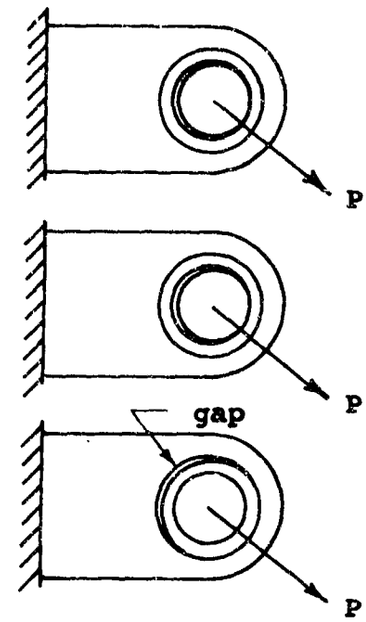

Description

Case 1 - Radial and tangential stresses exist between the lug and the liner. This corresponds to brazing the liner to the lug.

Case 2 - Only radial stress exists between the lug and the liner. This corresponds to rubber-cementing the liner to the lug.

Case 3 - Only radial compressive stress exists between the lug and the liner. This corresponds to a perfectly greased liner.

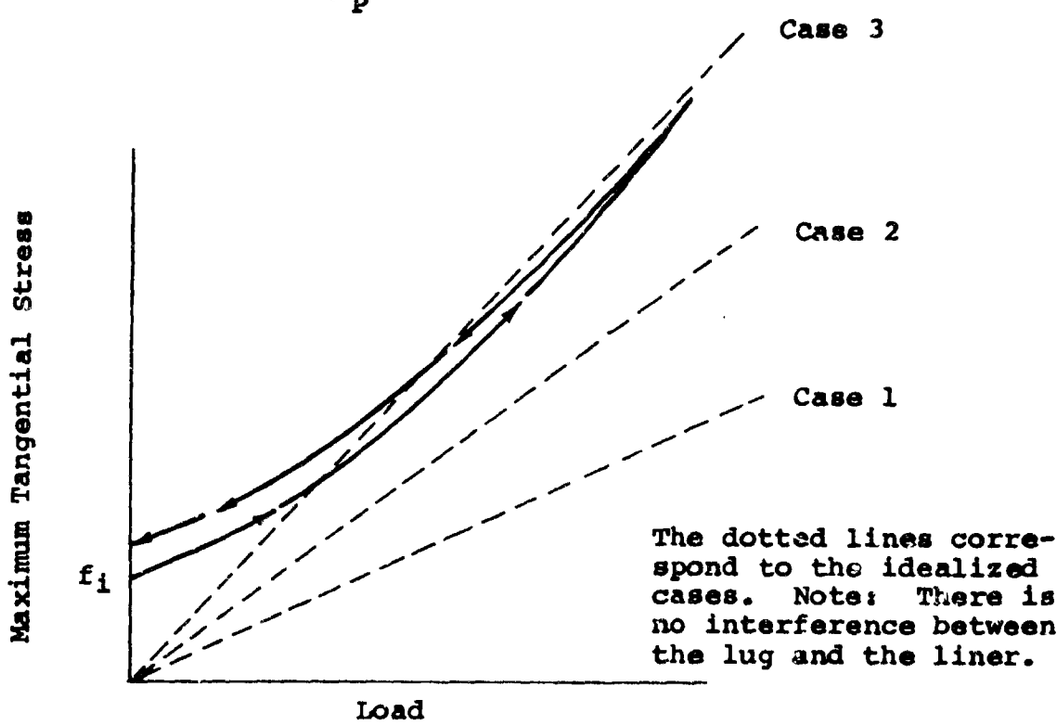

Figure 10. Stress Versus Load for Lug.

with a closely fitted pin. These idealized cases are shown because they assist in the explanation of the characteristic concave shape of the curve for the real lug. The concave shape has a very important effect upon the fatigue performance of the lug.

Consider the stress-versus-load curve as the load is increased gradually. Initially, at zero load, there is a high radial compressive stress caused by the interference fit between the lug and the liner. This radial compressive stress generates the lug preload stress, f_i, and also allows a tangential friction force to be developed. For low loads, the friction force prevents relative motion between the lug and the liner so that they act as a unit. Thus, the initial slope of the curve is parallel to the dotted line for Case 1. As the load is increased, the radial stress between the lug and the liner decreases on the side opposite to the direction of loading; and at some load, the friction force is not capable of preventing relative motion. Slipping then occurs, and the slope of the curve steepens and gradually approaches that of Case 2. At some higher load, the radial stress between the lug and the liner decreases to zero on the side opposite to the direction of loading. Then a gap opens. As the load is increased further, the gap widens, and the curve approaches the straight line for Case 3.

Figure 10 also shows the stress-versus-load curve as the load is decreased. In general, this curve is similar in shape to the curve for increasing load, but it is displaced because of friction between the lug and the liner. For the second and subsequent cycles of loading, the relationship tends to follow the decreasing load curve for the first cycle. However, the stress-versus-load relationship will gradually change during the life of the lug because of changes in the friction between the lug and the liner as fretting occurs. Such changes blur the stress-versus-load relationship and make it appear to be a band rather than a line.

The curve shown in Figure 10 becomes more convenient for quantitative description and more useful for comparisons between lugs if the load P is divided by the bearing, DT. The result is a curve of maximum tangential stress in the lug at the bore versus bearing stress. The same physical interpretations presented for the stress-versus-load curve also apply to the new curve.

Idealized Stress-Versus-Load Relationship

Figure 11 shows the idealized stress-versus-load relationship used herein. This relationship retains the essential concave shape of the actual stress-versus-load curve using only three straight line segments which are defined by six parameters. Three parameters depend only upon elastic stresses. These are:

K_{br} Stress concentration factor for tangential stress. It is the ratio of the maximum tangential stress in the lug at the bore to the average bearing stress, P/DT. K_{br} was calculated using the idealization shown in Figure 10, Case 3.

f_i Tangential stress in the lug caused by the initial interference fit between the lug and the liner. f_i was calculated using the idealization shown in Figure 10, Case 1.

f_g Bearing stress (P/DT) that causes the radial stress between the lug and the liner to become zero on the side opposite to the direction of loading. f_g was calculated using the idealization shown in Figure 10, Case 2.

The above parameters can be calculated from the geometry and the elastic properties of the materials. Procedures for making such calculations are described in detail in the section titled Analysis Procedure.

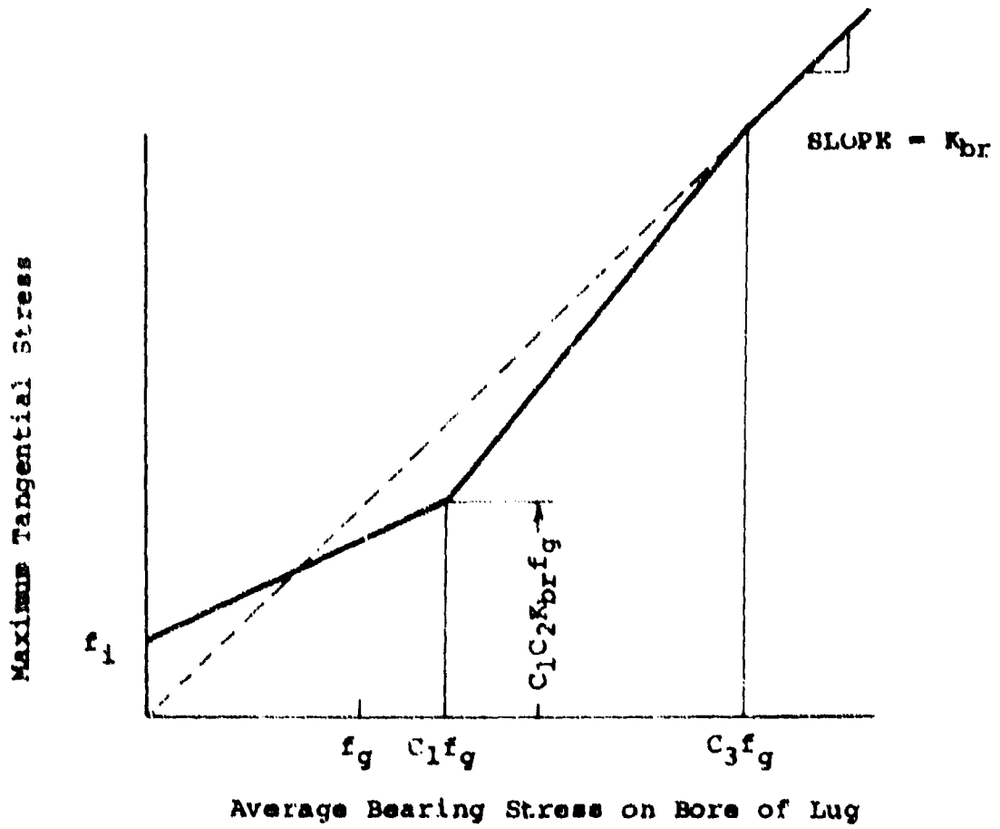

Figure 11. Idealized Tangential Stress Versus Bearing Stress for Lug.

The other three parameters, C_1, C_2, and C_3, control the concavity of the relationship. Their role can be seen in Figure 11. These parameters were determined from the results of fatigue tests performed in this program. It was found that

$$C_1 = 1.3$$

$$C_2 = 0.8 - (180 - \theta_p)(7i/D)^2$$

$$C_3 = 2.6$$

produced a good correlation of the fatigue test data with a reasonable Goodman diagram for the materials over a wide

range of test conditions for both steel and titanium lugs. The parameters C_1, C_2, and C_3 may be regarded as arithmetical tools for introducing concavity into the stress-versus-load relationship. However, it is also possible to attach physical meanings to these parameters. C_1 can be regarded as a factor which corrects the gap-forming load, f_g, for the effects of friction between the lug and the liner. C_2 and C_3 are also corrections for the effects of friction between the lug and the liner. In addition, C_2 contains a term $(180 - \theta_p)(7i/D)^2$ which was introduced to account for the observed fact that the presence of a press fit can prevent fretting at the location of calculated maximum stress and can cause the failure position to shift to another location where the calculated stresses are lower but the fretting is more severe. This effect appears to be more pronounced for axial loads than for loads at other orientations. For this reason, the factor $(180 - \theta_p)$ was introduced.

The use of parameters such as C_1, C_2, and C_3 to account for friction effects greatly simplifies the analysis because their introduction eliminates the need to calculate friction forces and slippage zones between the lug and the liner.

CORRELATION OF THE METHOD WITH TEST RESULTS

Modified Goodman Diagrams

The proposed method allows all tests to be compared on a common basis, namely, the computed tangential stress in the lug. If the computed stresses for all specimens of the same life and material were found to lie near a single line on a modified Goodman diagram, confidence would be established in the validity of the method. The line itself could be regarded as a characteristic strength property of the material, and the line could be used with the method to predict the fatigue strength for lug configurations for which no tests have been made. This section reports the results of such comparisons and establishes characteristic probable strengths.

In order to calculate stresses, it was first necessary to establish for each test the load that would cause failure in 10^7 cycles. The raw test data gave a survival load at which the specimen did not fail after 10^7 cycles, and a higher load which did cause failure after less than 10^7 cycles. One common procedure is to assume that the load for failure in 10^7 cycles is the average of the highest survival load and the failure load. Such a procedure does not acknowledge that the strength is higher for a specimen that nearly survives the

last 10^7 cycle step than for a specimen that fails soon after the failure load is applied. For this reason, an alternative procedure was used in this program. The load for failure at 10^7 cycles was determined by interpolation, using the procedure shown in Figure 12. The modest adjustments introduced had no effect on general strength levels but did tend to smooth the reduced data.

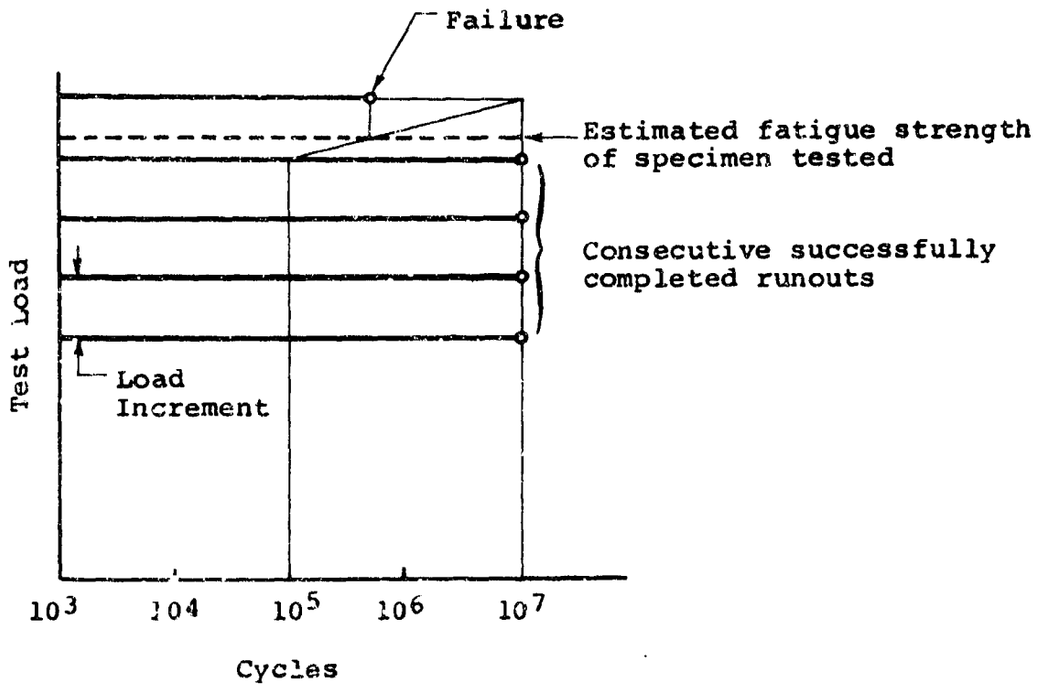

Figure 12. Interpolation Procedure Used to Find Load for Failure at 10^7 Cycles.

Using loads so determined, stresses were calculated for each test specimen that survived at least one step of 10^7 cycles. The method by which stresses were calculated is described in the section titled Analysis Procedure. A parametric study was made to determine the values for C_1, C_2, and C_3 that would produce reasonable lines on a modified Goodman diagram. The values $C_1 = 1.3$, $C_2 = 0.8 - (180 - \theta)(7i/D)^2$, and $C_3 = 2.6$ were selected as best and were used to prepare the modified Goodman diagrams shown herein.

Figures 13 and 14 show the modified Goodman diagrams for the tests of steel and titanium lugs, respectively. Each point shown in these figures corresponds to the calculated elastic stress for a fatigue test. It can be seen that the individual points for tests of the same type follow a definite pattern. They fall approximately on a line with a steep positive slope. This pattern is the natural consequence of scatter in a test procedure which maintains R = .1 for all load cycles. The pattern should not be interpreted to indicate that the material strength property is such that the alternating stress to cause failure increases with increasing mean stress. It is important to note that the test procedure has introduced a statistical bias into the data which makes it impossible to determine the slope of the Goodman line from a simple, straight-line, least-squares fit to the test points. Instead, the slope of the line must be established from previous knowledge of the material behavior. The slopes of the mean Goodman lines shown in Figures 13 and 14 were selected using the typical constant-life fatigue diagrams for AISI 4340 steel (bar) and annealed Ti-6Al-4V alloy (bar) shown in reference 3. The slopes shown in Figures 13 and 14 may at first appear to be too flat; however, their flatness is reasonable when one considers that maximum stresses on a section are plotted rather than an average stress, as done in reference 3.

Allowable Stresses

The calculated stresses for the tests were interpreted to provide estimates of probable fatigue strength for use in the proposed method for lug analysis. This section describes the statistical procedures used and presents the strength estimates. The objective of the statistical analysis was to establish one-sided lower tolerance limits for fatigue strength at 10^7 cycles. Such limits have the following property: With a confidence γ, at least p percent of the population will have a strength greater than the one-sided lower tolerance limit, $\bar{x} - ks$, where $\bar{x}$ and s are computed from a sample size of n.

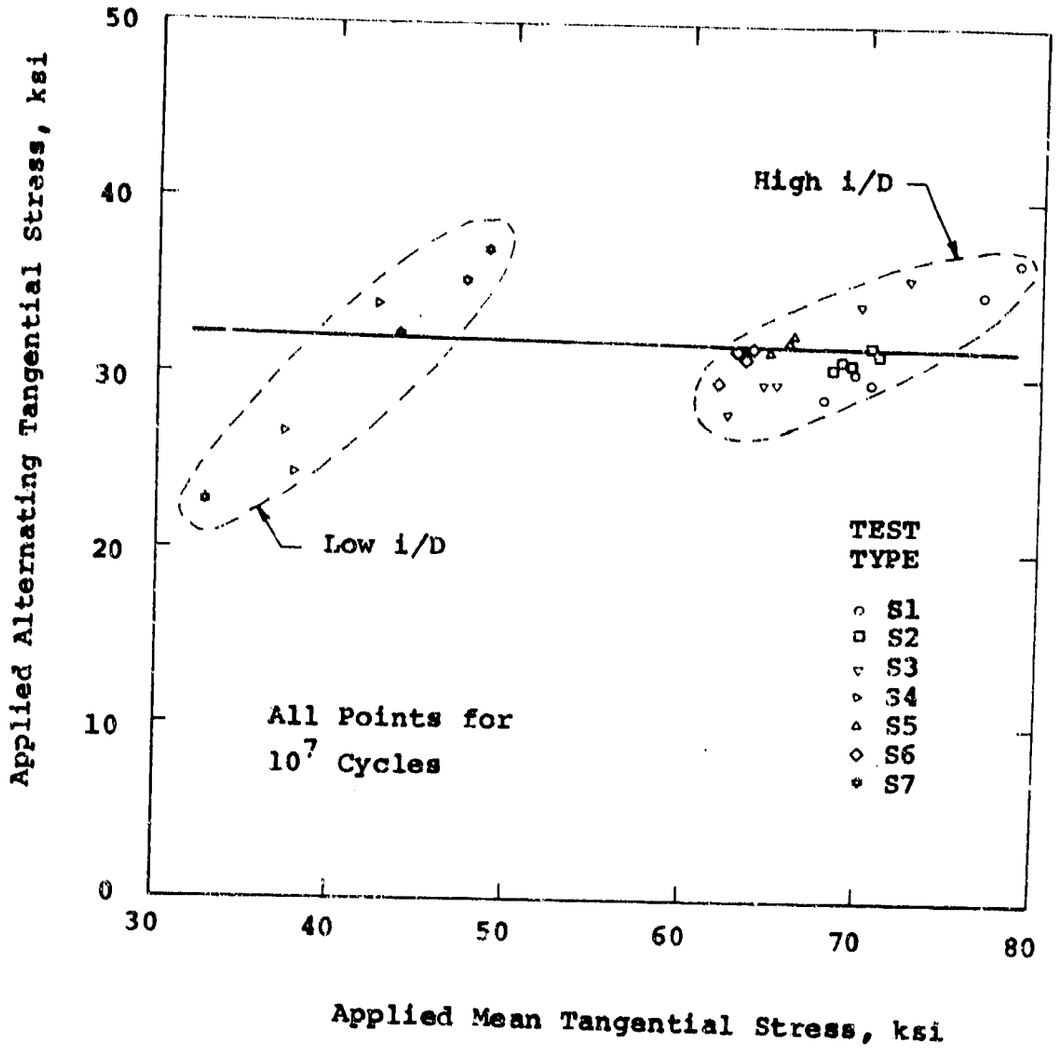

Figure 13. Modified Goodman Diagram for Tests of Steel Lugs.

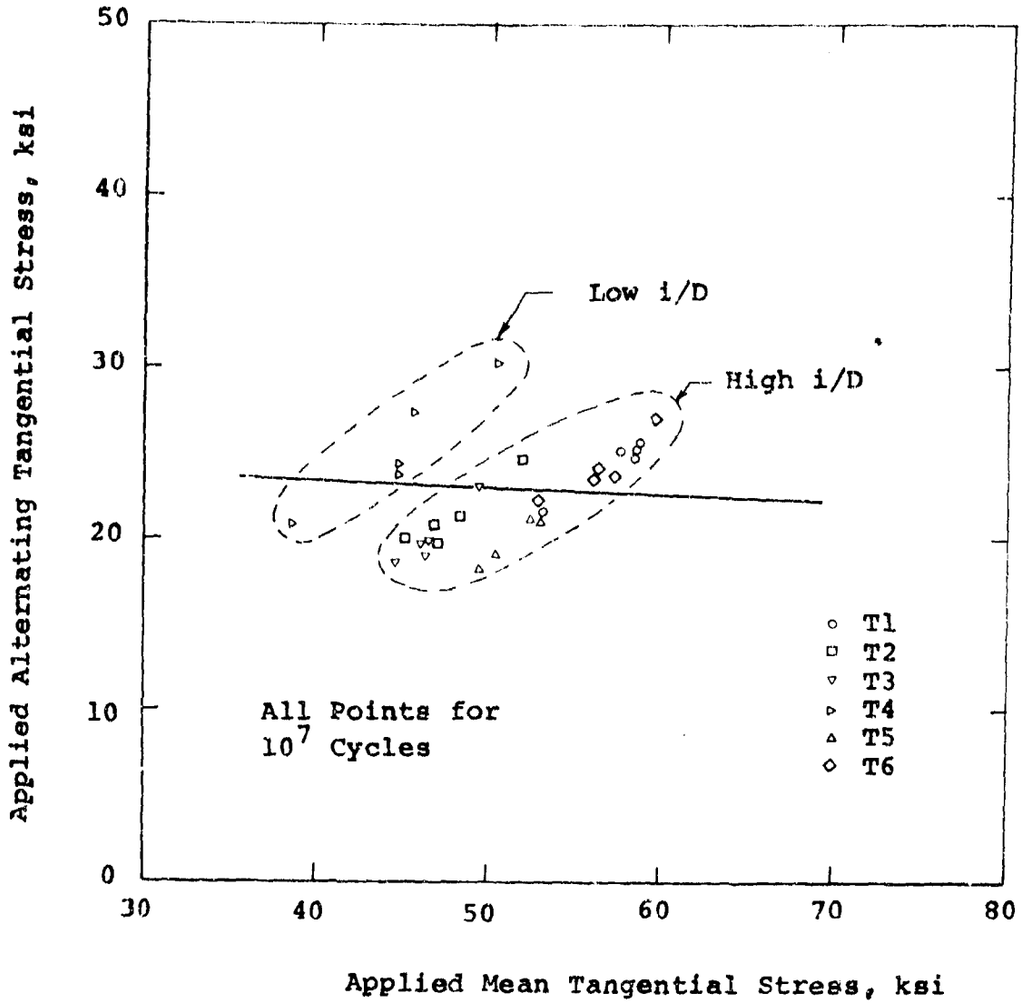

Figure 14. Modified Goodman Diagram for Tests of Titanium Lugs.

An inspection of Figures 13 and 14 shows that the calculated stresses for the tests which used a high interference demonstrated less scatter than those for low or medium interference. For this reason, the lug tests were considered to be samples from four different populations:

Steel lugs with low i/D
Steel lugs with high i/D
Titanium lugs with low i/D
Titanium lugs with high i/D

Estimates were made for each population using the assumption that at a common mean stress, the logarithm of the fatigue strength is normally distributed. The test alternating stresses were transferred to a common mean stress (70 ksi for steel lugs; 45 and 55 ksi for titanium lugs with low and high i/D, respectively) using the slopes for the modified Goodman line shown in Figures 13 and 14. The sample mean, $\bar{x}$, and standard deviation, s, were calculated for each sample using:

$$\bar{x} = \frac{1}{n}\sum x_i, \text{ and } s = \left[\frac{\sum(x_i - \bar{x})^2}{n - 1}\right]^{1/2}$$

where x_i = $\log_{10}$ test alternating stress

n = sample size

$\sum$ = summation from 1 to n.

One-sided tolerance limits were calculated for the sample from each population using $\bar{x} - ks$, where k is a one-sided tolerance factor which can be found in reference 1.

The test data and the tolerance limits are shown graphically in Figures 15, 16, and 17. The individual tests in these figures were positioned using the method of median ranks. This method places the test points in the median expected positions for all possible samples of the same size taken from the population. The tolerance limits in Figures 15, 16, and 17 are shown to low probabilities of failure, far beyond the test data. It is important to note that such estimates contain an element of conjecture. They are accurate only if the population is normally distributed, as assumed. For the tests reported herein, this assumption appears to be reasonable; however, the true distribution cannot be known without a much larger number of tests. The justification offered for

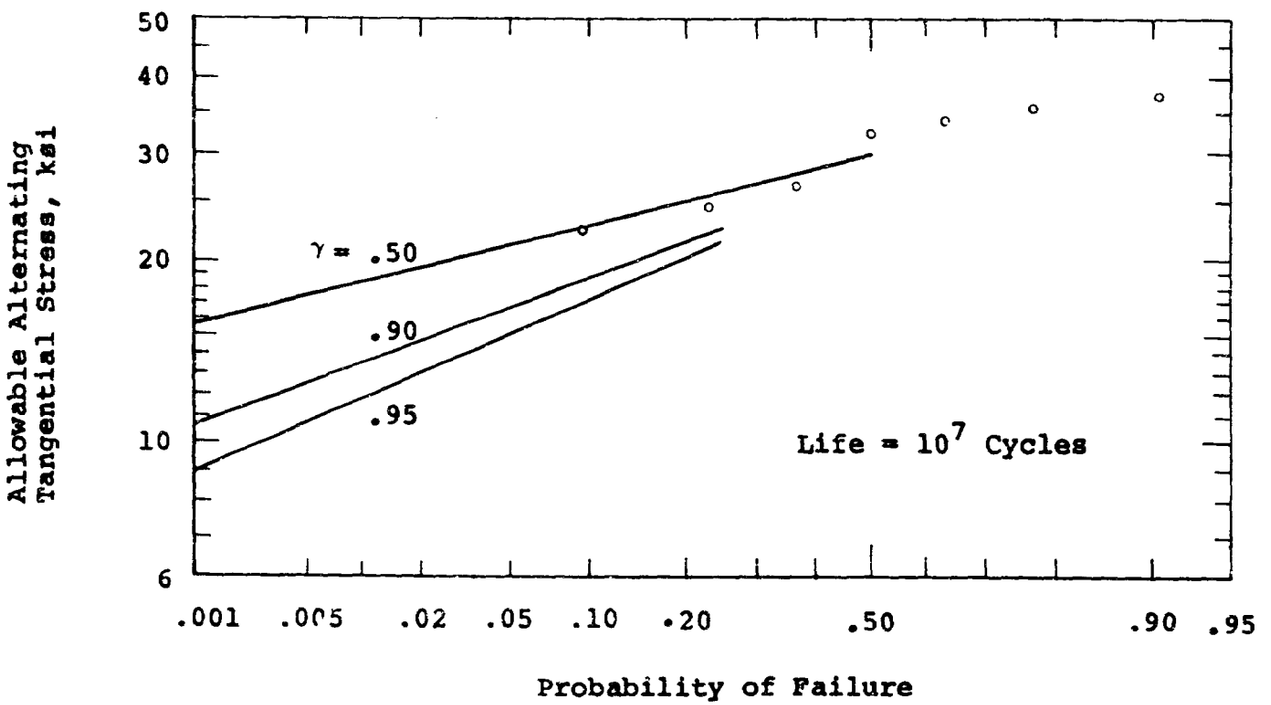

Figure 15. Stress Versus Probability of Failure for Steel Lugs With Low i/D.

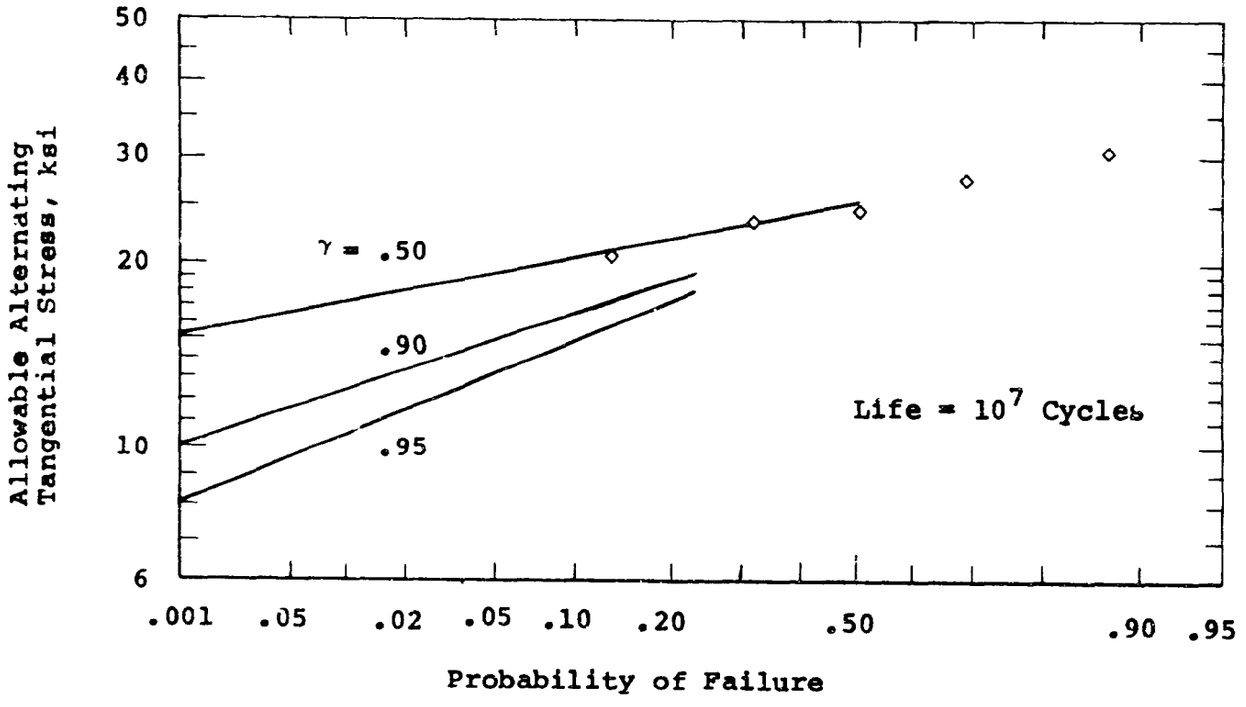

Figure 16. Stress Versus Probability of Failure for Titanium Lugs With Low i/D.

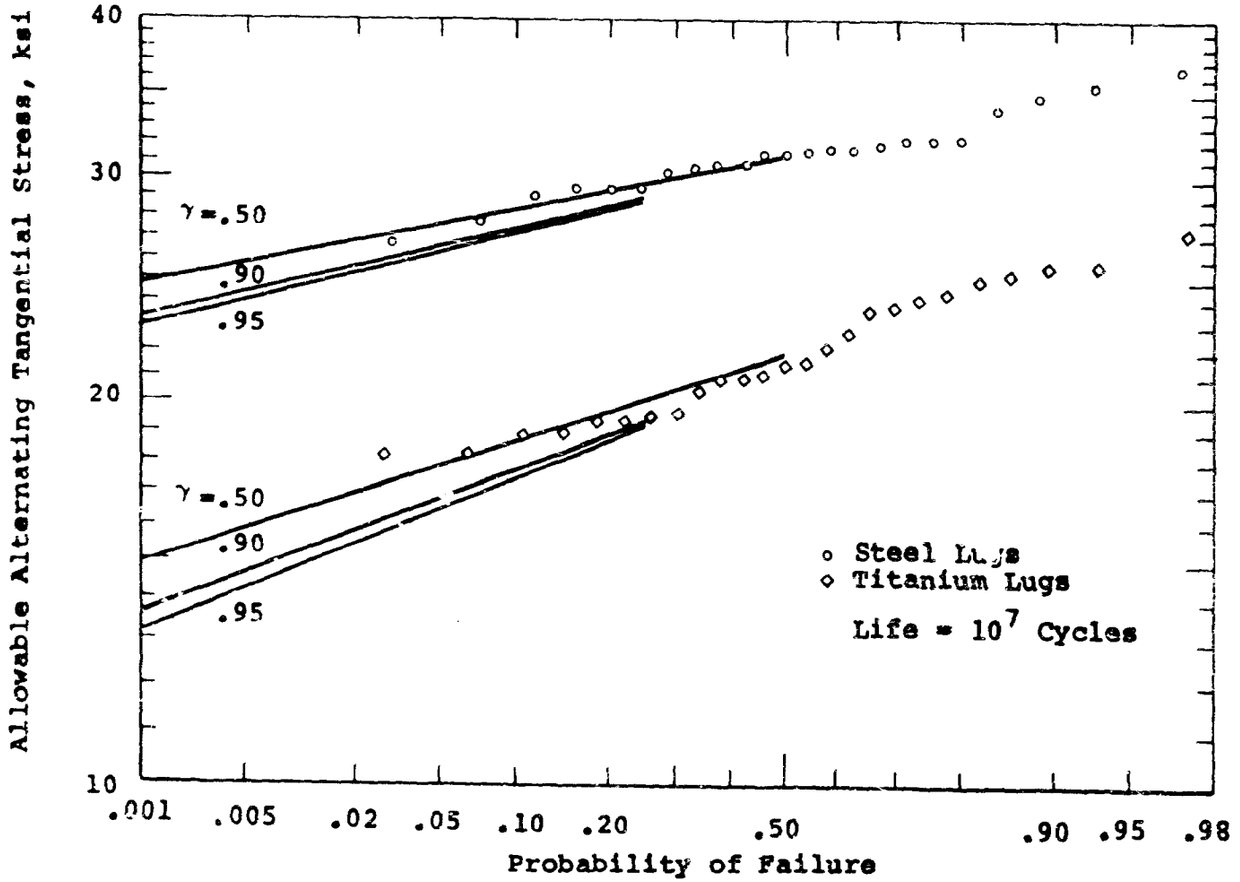

Figure 17. Stress Versus Probability of Failure for Lugs With High i/D.

extending the estimates to low probabilities of failure is that there is a need for lug designs with low probability of failure, and in lieu of statistical precision this method offers a logical adjustment of available data.

The allowable stresses for typical probabilities of failure used in lug design are summarized in Table V.

TABLE V. ALLOWABLE ALTERNATING TANGENTIAL STRESSES (KSI) FOR 10^7 CYCLES.

		Steel		Titanium	
P	γ	Low i/D	High i/D	Low i/D	High i/D
.50	.50	29.8	31.3	25.1	21.8
.10	.90	18.7	27.5	16.6	17.7
.001	.90	10.6	23.3	10.0	13.6

The allowable alternating stresses in Table V are applicable in the strictest sense only to a mean stress of 70 ksi for steel lugs and 45 ksi and 55 ksi for titanium lugs with low and high i/D, respectively. However, in view of the flatness of the modified Goodman diagrams shown in Figures 13 and 14, the allowable alternating stresses in Table V may be regarded with engineering accuracy as independent of mean stress if the maximum stresses are within the range of those encountered in this test series, 115 ksi for steel and 85 ksi for titanium.

DESIGN CHARTS

In many cases, a designer can make a direct selection of lug proportions to achieve a desired load capacity by using the charts in Figures 18 through 23. These charts also provide a picture of attainable performance because the parameters were selected to cover the range of practical interference fits and probabilities of failure. In all 24 charts are presented: 12 for steel lugs, and 12 for titanium lugs. The materials correspond to those tested in this program, namely:

AISI 4340 alloy steel, heat treated to F_{tu} = 175 ksi

Ti-6Al-4V alloy titanium, annealed, F_{tu} = 130 ksi

Both materials were shot-peened with shot size SAE 330, intensity 12-14A2. For each material, charts are presented for:

3 directions of load	θ_p = 0°, 45°, 90°
2 probabilities of failure	p = .10, 001
2 levels of interference	
for steel	i/D = .001, .004
for titanium	i/D = .001, .005

For all curves, a steel liner with D/d = 1.184 was used. This value corresponds to that used in the tests.

The solid-line curves in the design charts were prepared using the proposed method for calculating fatigue strength and the alternating stress allowables from Table V. The solid-line curves were terminated at a maximum calculated stress of 115 ksi for the steel lugs and 85 ksi for the titanium lugs. These stress levels correspond approximately to the maximum values experienced in the test program. It is noted that in the high-press-fit cases, the solid-line curve is a straight, horizontal line. This corresponds to the fact that a maximum steel stress of 115 ksi or titanium stress of 85 ksi was still on the initial slope of the stress-versus-load relationship shown in Figure 10. For the low-press-fit cases, the solid-line curve has an S-shape. This is a consequence of progression over the slopes of the stress-versus-load relationship. The design curves shown herein were faired slightly to account for the fact that the transition from one slope to another is, in reality, smooth rather than abrupt.

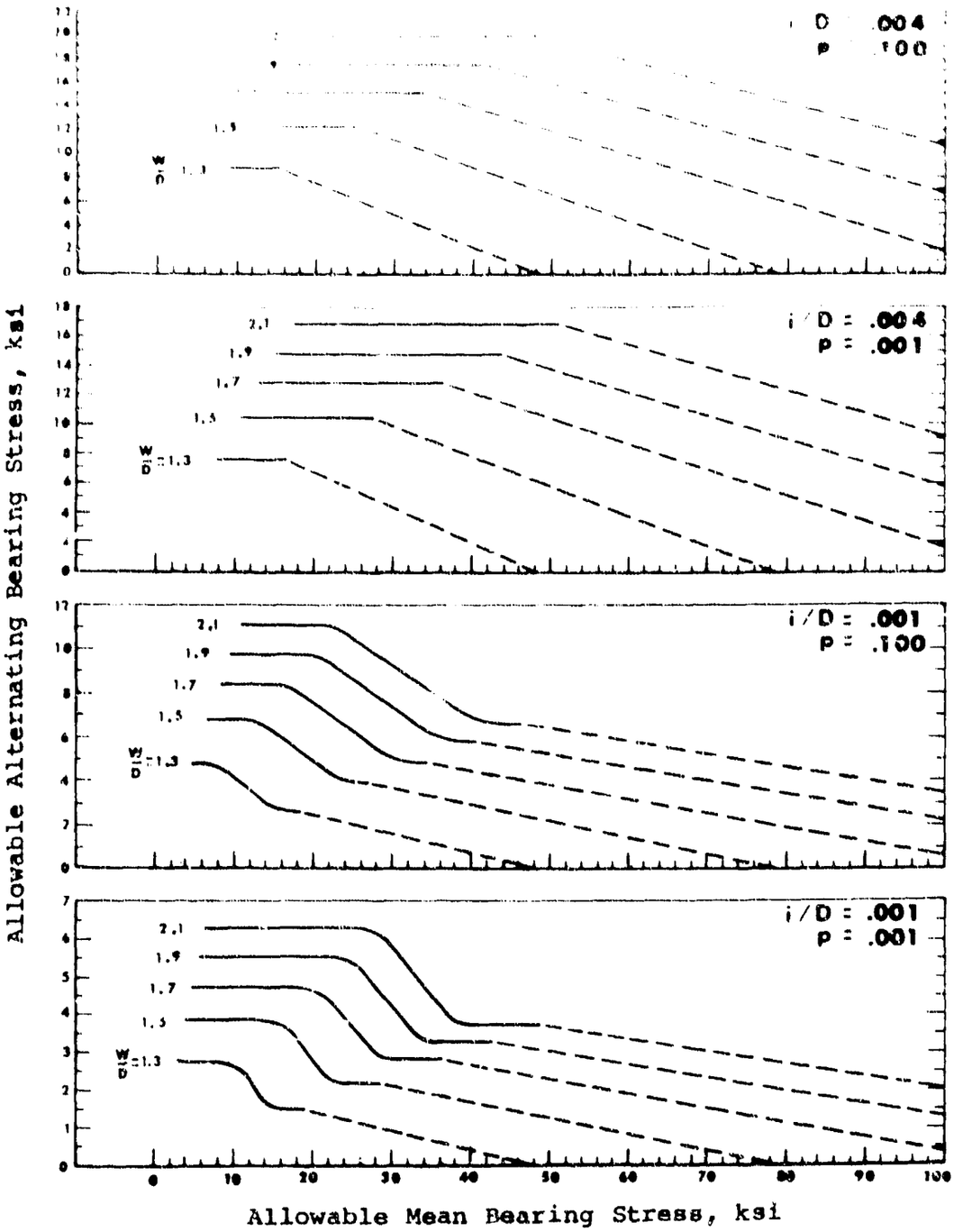

Figure 18. Fatigue Strength of Steel Lugs for $\theta_p = 0^o$.

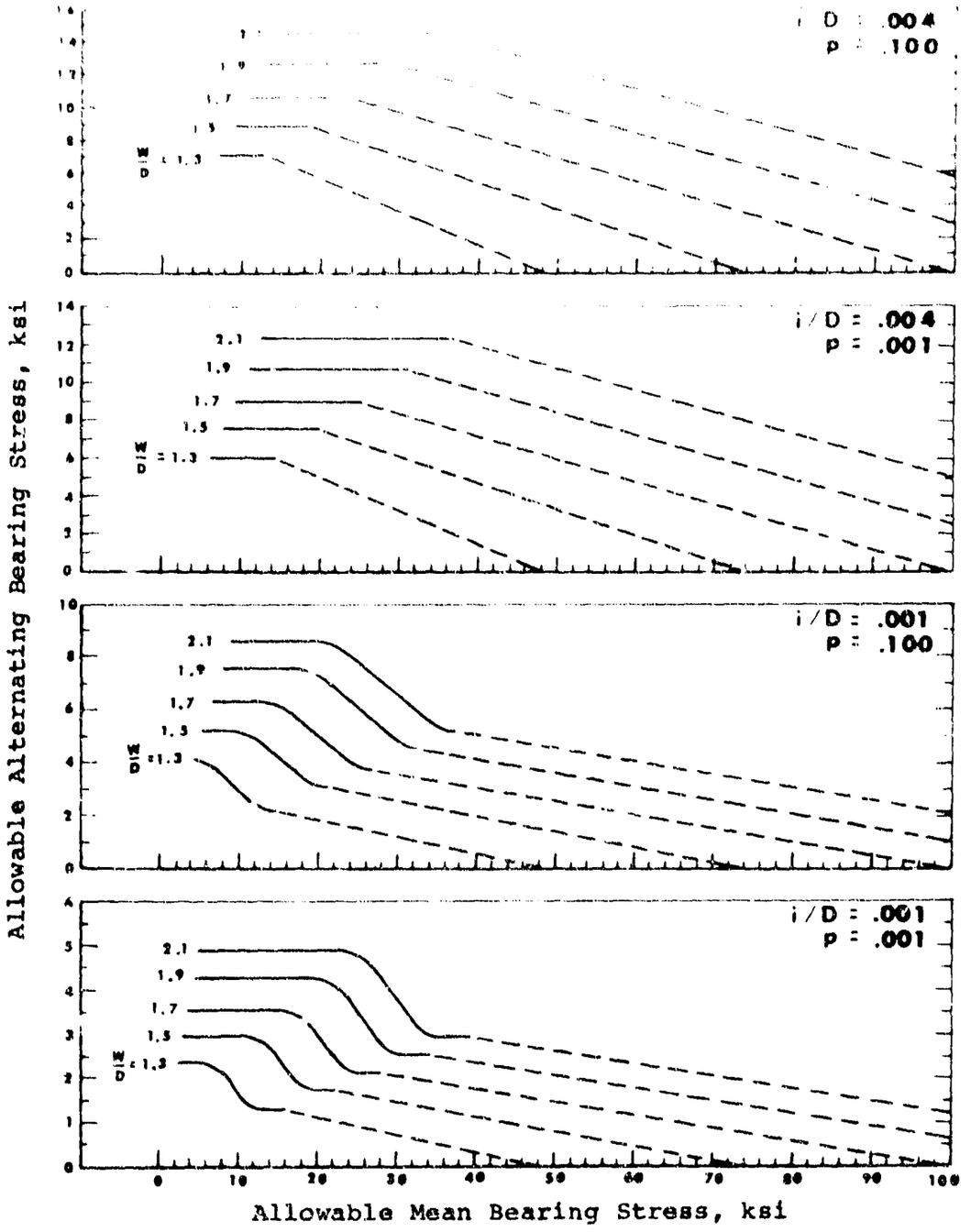

Figure 19. Fatigue Strength of Steel Lugs for $\theta_p = 45^o$.

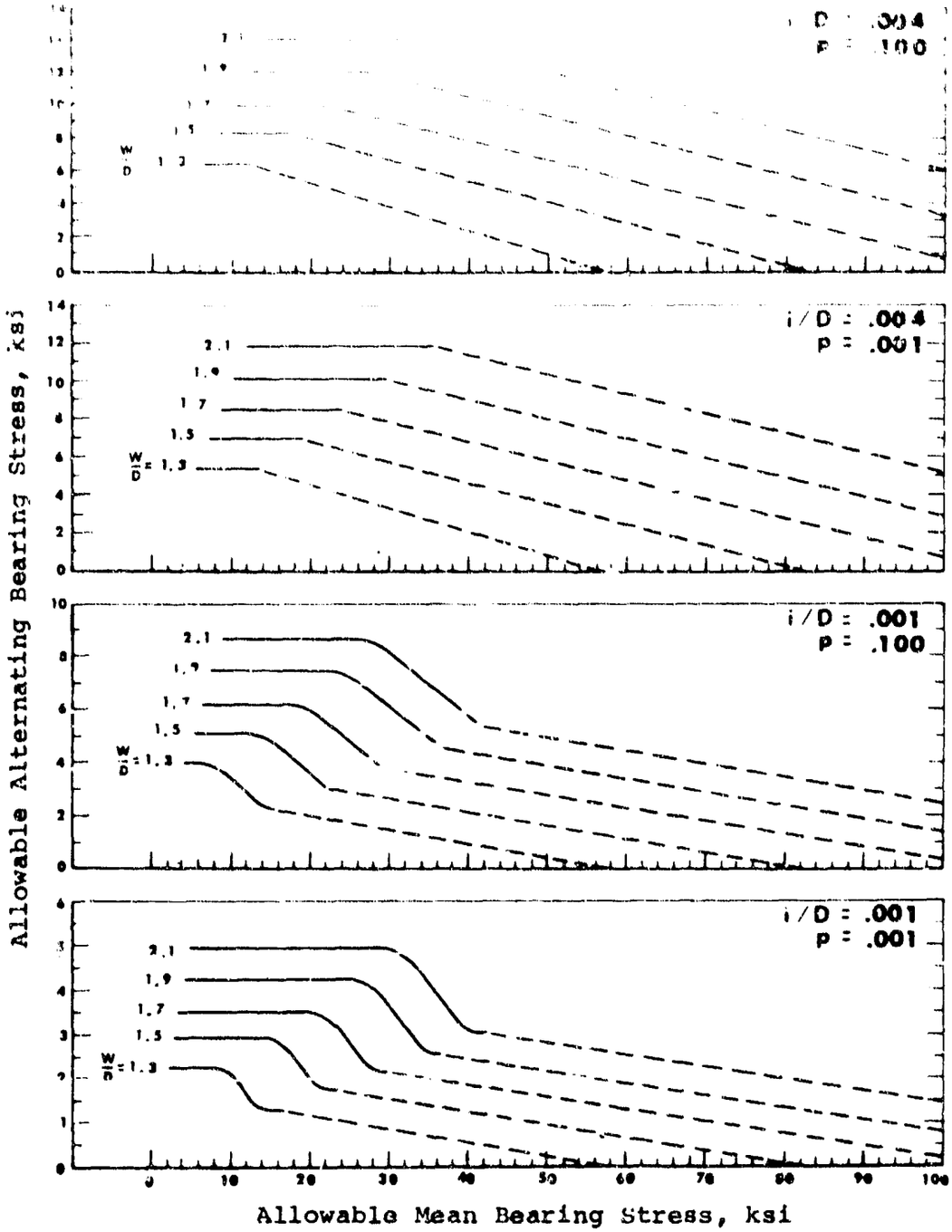

Figure 20. Fatigue Strength of Steel Lugs for $\theta_p = 90^o$.

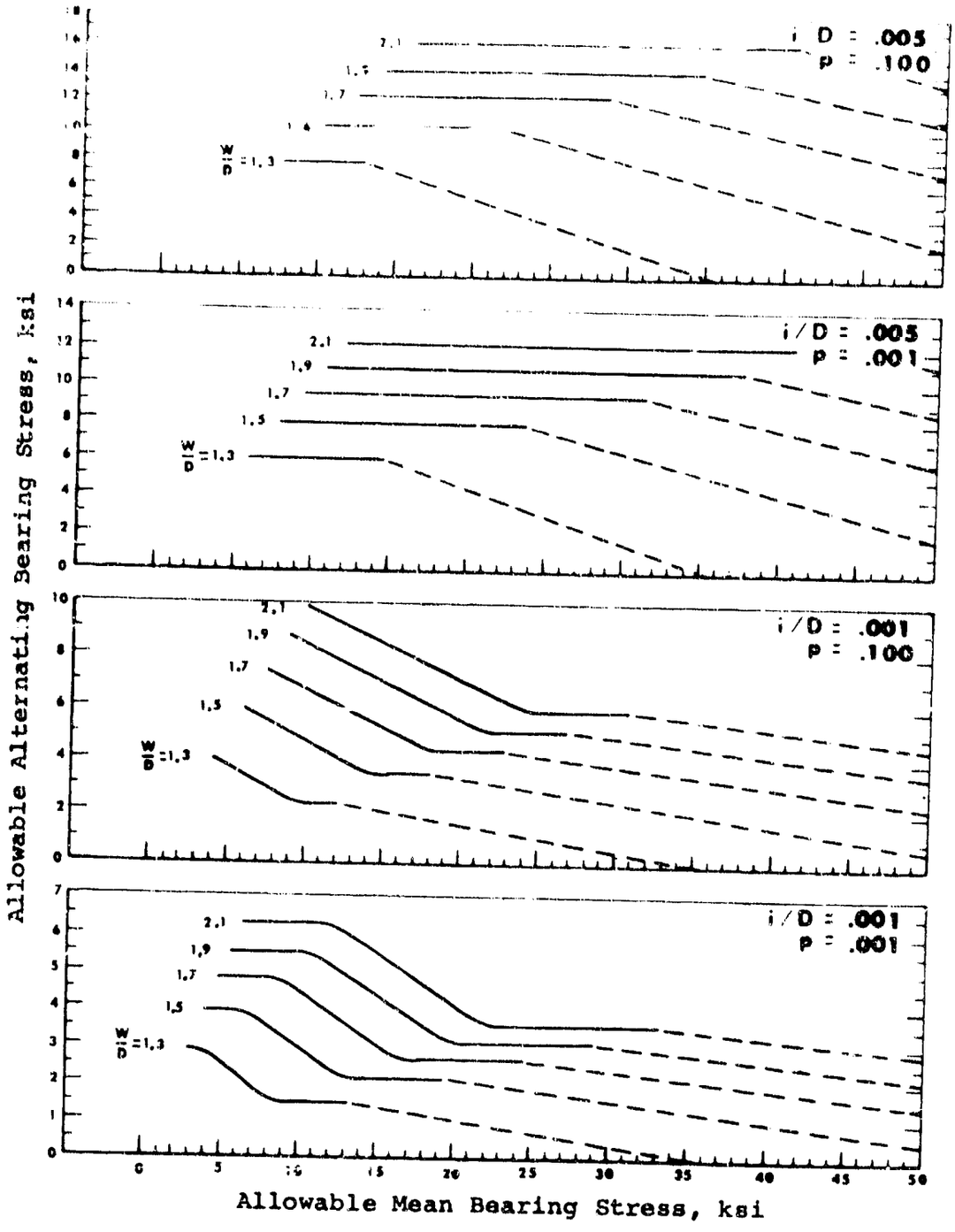

Figure 21. Fatigue Strength of Titanium Lugs for $\theta_p = 0^o$.

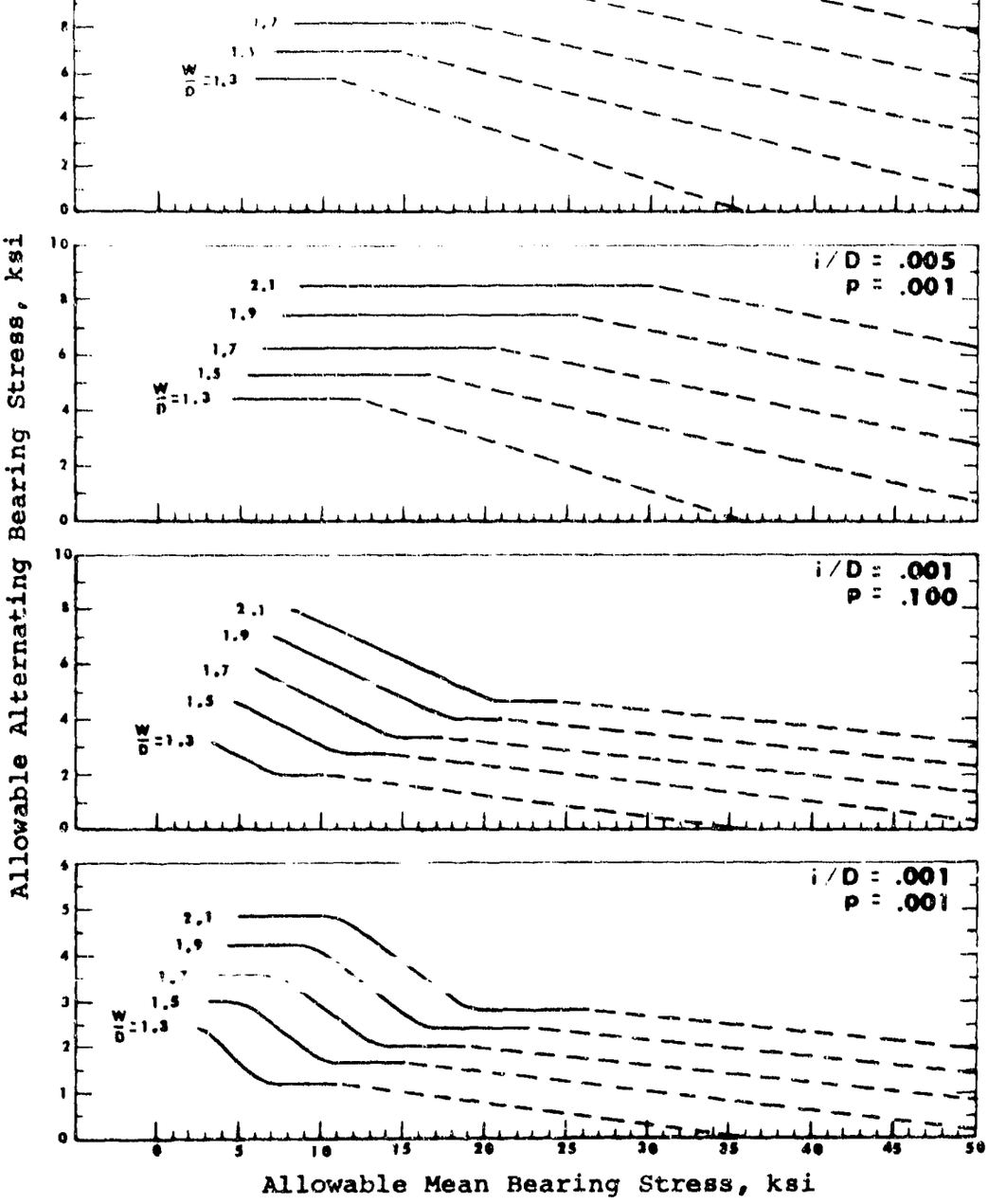

Figure 22. Fatigue Strength of Titanium Lugs for $\theta_p = 45^o$.

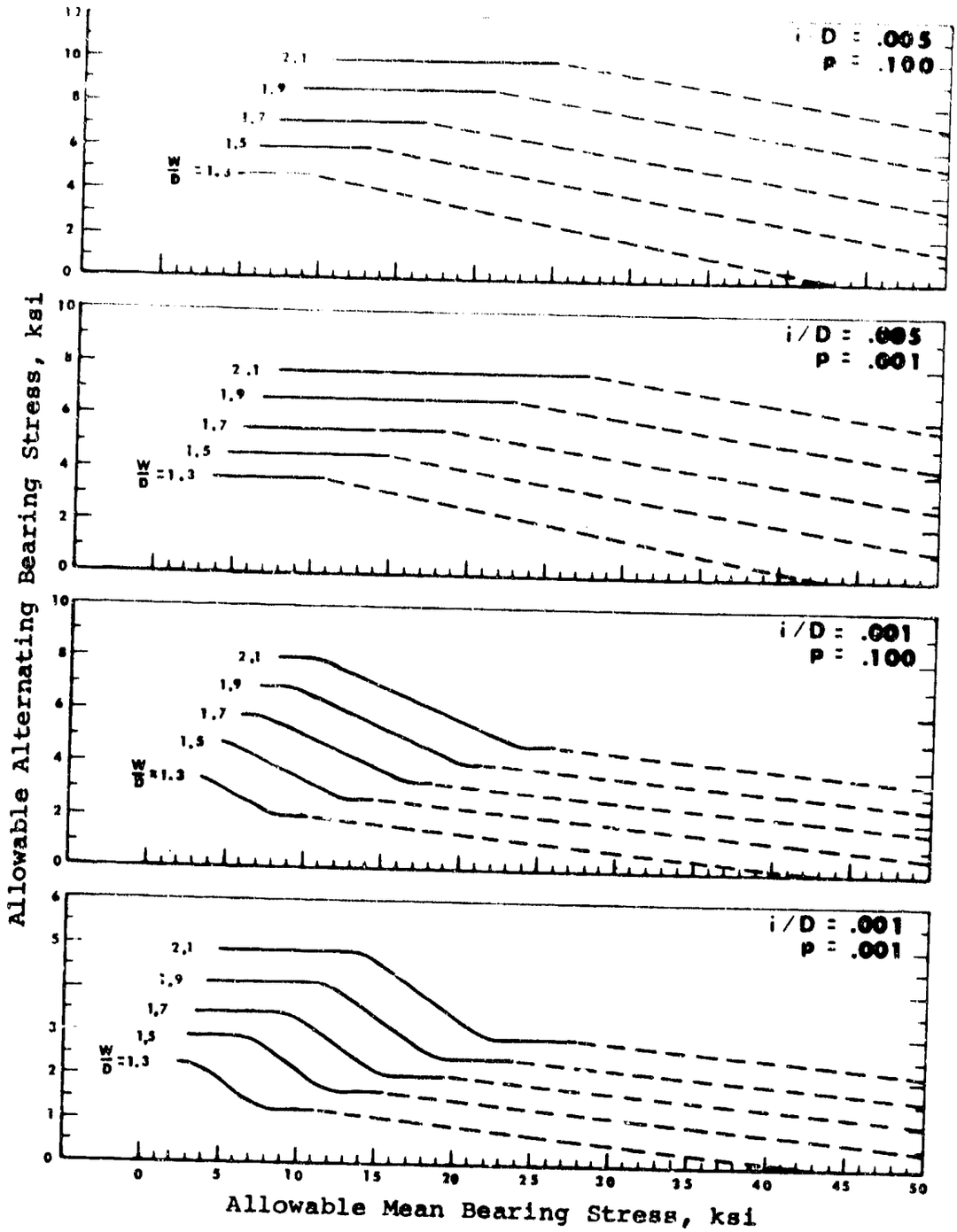

Figure 23. Fatigue Strength of Titanium Lugs for $\theta_p = 90^\circ$.

The dotted-line portions of the curves are simple straight-line connections to the ultimate strength, which was calculated using the method of Melcon and Hoblit, reference 2. It is important to emphasize that the dotted portions of the curves are conjectured performance. Only the end points of the dotted curves have a basis in test experience. The following example illustrates the use of the design curves.

Given: A steel lug is required to support an axial load of 50 kips ±10 kips for 10^7 cycles. A liner with high interference fit can be used. The diameter of the pin is 1.5 inches. The thickness of the lug is .75 inch.

Required: Width of lug to provide a probability of failure of less than p = .001.

Solution:

Use i/D = .004
D/d = 1.184
Then i = .0071 in.
D = 1.776 in.
DT = 1.125 sq. in.
P_{mean}/DT = 50/1.125 = 44.4 ksi
P_{alt}/DT = 10/1.125 = 8.88 ksi
From Figure 18, W/D = 1.58
Therefore, use W = 2.81 inches

The reader is cautioned to note that several scales are used for the alternating stress in the design charts. These scales were selected to produce easy-to-read curves and a compact presentation. However, the use of different scales for the ordinate and abscissa causes a line of constant stress ratio R to have a different slope than customary on a conventional constant-life diagram. All curves shown in the design charts start at R = 0. Extrapolation of the curves to lower mean stresses than shown in the charts would correspond to loadings which reversed in sign (from tension to compression) during each load cycle. The performance of lugs under such conditions has not been investigated in this program. It is anticipated that lug performance could fall off, particularly if the pin permitted dynamic loads to develop. A possible relationship is shown in Figure 24.

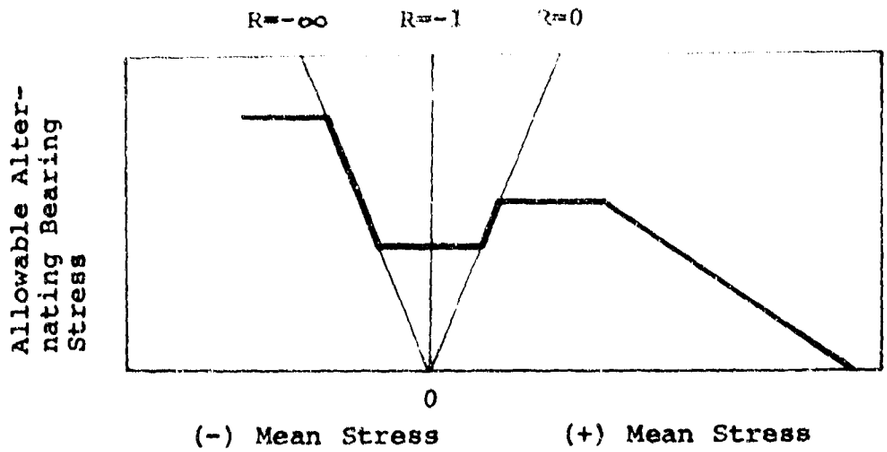

Figure 24. Anticipated Appearance of Constant-Life Diagram for Lug, Including Load Reversals.

INTERACTION EQUATION FOR OBLIQUE LOADS

In reference 2, Melcon and Hoblit described the static strength of obliquely loaded lugs using the interaction equation

$$R_a^{1.6} + R_t^{1.6} = 1$$

where

$$R_a = \frac{\text{axial component of load}}{\text{allowable axial load}}$$

$$R_t = \frac{\text{transverse component of load}}{\text{allowable transverse load}}$$

In the present program, procedures for analysis are presented which permit the direct calculation of stresses for oblique loadings without use of an interaction equation. However, it is interesting to note that the interaction equation appears to be approximately correct for fatigue strength as well as for static strength. The equation was used to predict the allowable alternating load for $\theta_p = 45^o$ with a load ratio R=0 for the cases shown in the design charts. It was found that the differences between the analysis method and the interaction equation covered a range of -8.5 to +4.4 percent with an average difference of less than 1 percent.

REVIEW OF LUG LITERATURE

The present program is a unique effort combining theoretical and experimental work to provide a unified and practical solution to the problem of design of fatigue-loaded lugs. It has been preceded by many individual efforts. Contributions from the fields of theoretical mechanics, photoelasticity, strain measurement, and fatigue tests can be readily found in the literature, and much of the prominent work is listed in the references of this report. The theoretical and photoelastic work has the advantage of providing a complete stress distribution throughout the lug so that location and magnitude of maximum stresses are known. However, the choice of the proper failure theory and the influence of fretting, friction, and interference fit are factors that tend to make the applicability of these results to fatigue-loaded metal parts less direct than is desirable. Fatigue testing, not supported by a generalized theory, yields specific information on isolated configurations but not a unified approach to the problem of predicting actual lug fatigue performance. The literature reports many prior efforts that have contributed to the present understanding of the subject, some of which are reviewed in the following discussion.

Frocht, in reference 4, presents a compilation of photoelastic and strain measurement data for axially loaded lugs ($\theta_p = 0$) that show excellent agreement and complement each other well. The figures presented in this source have been widely referenced and used in the design of single pin connections. Figure 6.12 of that reference shows stress concentration factor, $f_{max}/f_{average}$, plotted versus the ratio of hole diameter to lug width, and the basic curves are reproduced here as Figure 25. Also shown in Figure 25 for comparison purposes are the calculated stress concentration factors derived in the present program. It will be noted that there is excellent agreement at the higher edge distances, $W/D = 1.69$ and 2.1; but at the lower value $W/D = 1.3$, the notch factor calculated in this program falls slightly below Frocht's curves. It should be noted that this point coincides with the limit of data available in that reference. The actual curves are terminated at a notch factor slightly less than 2.0 and exhibit a downward slope for lower edge distance lugs. Considering the extremes of lug geometry where hole diameter approaches lug width ($D/W = 1.0$), the notch factor for this case is of some interest since it would assist in locating the curve for lugs of very low edge distance. It may be reasoned that an extremely thin strap of material surrounding a hole that was filled by a neatly fitting pin could not have a significant stress gradient across its thickness.

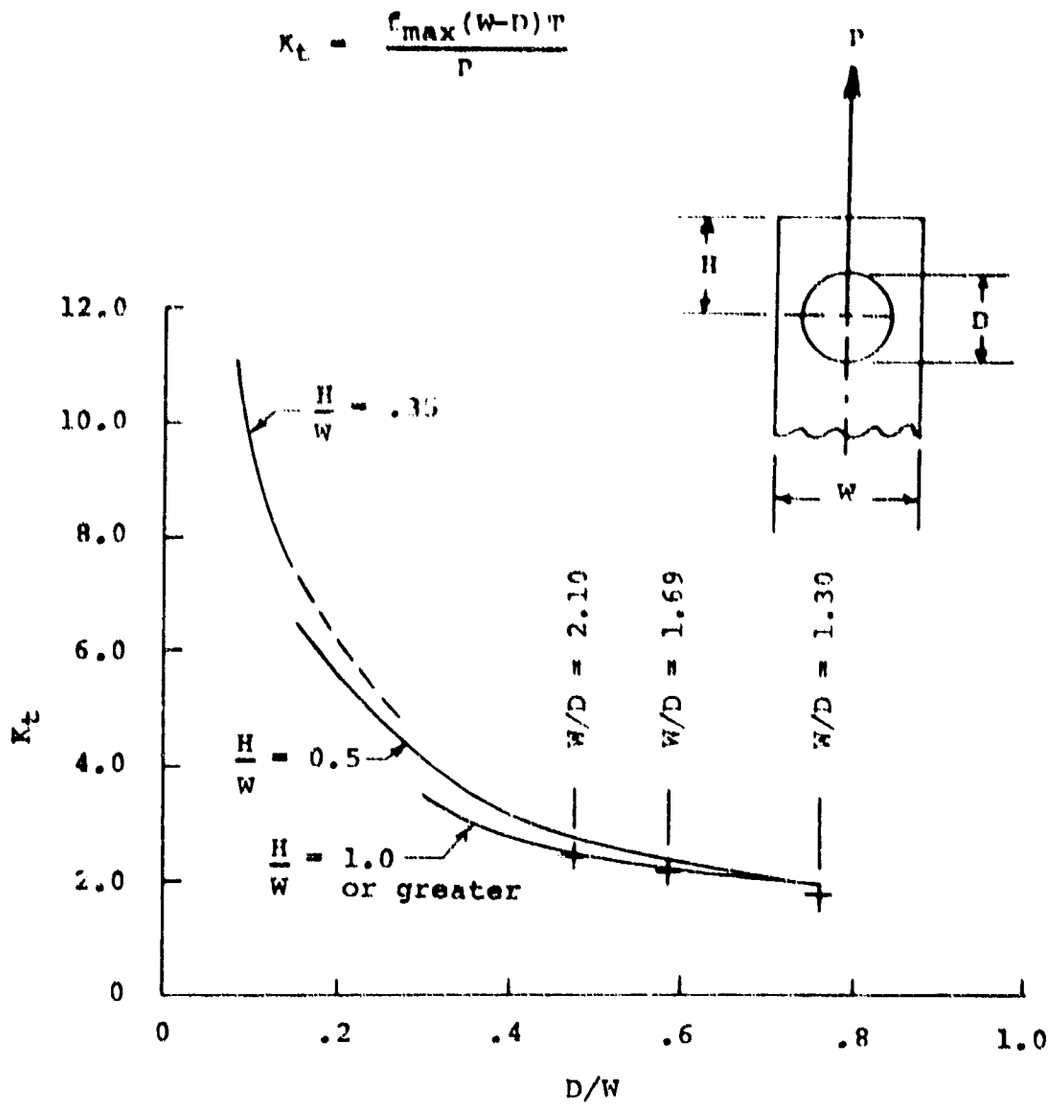

Figure 25. Stress Concentration Factor K_t Versus the Ratio of Diameter to Width.

However, some analyses have indicated apparent notch factors as high as 2.0 for the limiting case of D/W = 1.0. The existence of this anomaly is apparent in a review of the literature.

Reference 5 reproduces Frocht's curves but elevates them in the low edge-distance range. This modification is supported by an empirical formula for the case of an unloaded hole in a narrow tension strip which yields a notch factor of 2.0 for D/W = 1.0. Reference 6 reproduces Frocht's curves but lowers them in the low edge-distance range, apparently sloping toward a notch factor of 1.0 at D/W = 1.0. This adjustment apparently results from an assumption that there would be very limited stress gradients for extremely thin lugs. If the notch factors calculated in the present study were extrapolated to D/W = 1.0, they would indicate a notch factor greater than 1.0 and less than 2.0, with a likely value approximately 1.5. It is concluded that the notch factors calculated herein for axially loaded lugs are consistent with data in the literature.

References 7 and 9 report the results of photoelastic investigations of lugs subjected to nonaxial loading through single pins. The reference 7 study includes the influence of interference fit and concludes that the stress concentration factor based upon shear stress continues to increase and is a maximum for 90° loading. However, many individual data points presented in that report show a slight decrease for the final 90° point, particularly for the higher levels of press fit investigated. Reference 8 shows the variation of apparent stress concentration factor (based on maximum observed fringe order) versus angle of loading for lugs without interference fit and shows an almost linear variation with angle of loading. Separation of principal stresses was not attempted, and it is therefore assumed that the maximum fringe count again represents a measure of shear stress. The data presented in reference 8 show a smooth variation with a maximum stress concentration factor for a 90° loading. The calculations presented in the Analysis Procedure section of this report yield a variation of stress concentration factor with angle of load application which peaks in the range of 60° to 75° orientation, as shown in Figure 28, and is slightly lower at the 90° position. This figure is based on a stress concentration factor which considers only normal stress tangential to the lug bore. This is the stress that has been found to be most directly related to the fatigue failure mode and location observed in this program.

Lambert and Brailey present in reference 9 a study of the effect of the coefficient of friction between pin and lug on stress distribution in the lug. Their work is based on a photoelastically determined shear stress concentration factor and clearly illustrates the occurrence of slip between lug and liner on the first cycle of loading. Thereafter, residual shear tractions are present during subsequent cycles of loading. Further slip beyond the first cycle was not observed in this photoelastic study, although the persistent appearance of fretting in the bore of fatigue-loaded metal lugs with or without interference-fitted liners demonstrates its presence at least on a minute scale. The fact that the friction introduces shears to the surface of the lug bore at approximately the location of the maximum shear stress provides an additive influence that may not be of comparable significance in generating fatigue failures in metal lugs. The role that relative motion and friction play in establishing fretting and debris in the lug bore is thought to be of far greater significance than its influence on stress distribution.

In reference 10, Ligenza suggests the existence of an optimum interference fit for reduction of cyclic stresses in lugs. The optimization results from a balance of the increase in steady stresses against the reduction in cyclic stresses, and since the latter are of far greater significance, relatively high levels of steady stress usually result. For the steel and titanium lugs treated in this program, it was found that the level of interference was limited by practical considerations of attainable thermal size change even when using liquid nitrogen to chill the liners. Therefore, in this case the optimum was the maximum interference possible without heavy force fitting of the liners which would risk damage to the lug bore. For lugs of lower modulus or liners of substantially heavier wall, it is possible that steady stresses would limit the interference; however, such a study was beyond the scope of the present program.

ANALYSIS PROCEDURE

ELASTIC STRESSES

This section gives values for K_{br}, f_1, and f_g and describes how the data were obtained. With the data herein, the stresses can be calculated for a wide range of lug geometries and loadings.

A computer calculated elastic stresses and deformations within lugs for several geometries and loadings. Volume II of this report describes the computer program in detail and gives complete examples of its application to lug analysis. The computer program used the finite-element method, which analyzes the lug as an assembly of small elements. The attraction of this method for lug analysis is its great versatility; it is capable of analyzing a lug of any geometry for any direction of loading in the plane of the lug. The method is approximate because it places restrictions upon the form of the strains that can occur within the elements. However, comparisons of finite-element solutions with known exact solutions have shown that the stresses and deflections from a finite-element analysis are nearly correct if the elements are small in relation to the strain gradients. Such is the case for the solutions reported herein. Figure 26 shows the idealization of the lug assembly for finite-element analysis. This idealization has 266 elements that meet at 258 node points. The computer output includes the stress in each element and the deflection at every node point. An important feature of this idealization is the system of radial links. One set of links connects the pin to the liner; another set connects the liner to the lug. These links perform two functions that are essential for a true representation of the behavior of a real lug:

1. They allow tangential motions to occur between the pin, the liner, and the lug.

2. They allow radial gaps between the liner and the lug to be created or eliminated by the appropriate omission or retention of the radial links.

To obtain the data herein, the computer analyzed two types of loading: that from a mechanical force applied to the pin and that from an interference fit between the liner and the lug. The interference fit was introduced by specifying an appropriate temperature rise for the liner. The mechanical force was introduced by specifying a concentrated force at the center of the pin.

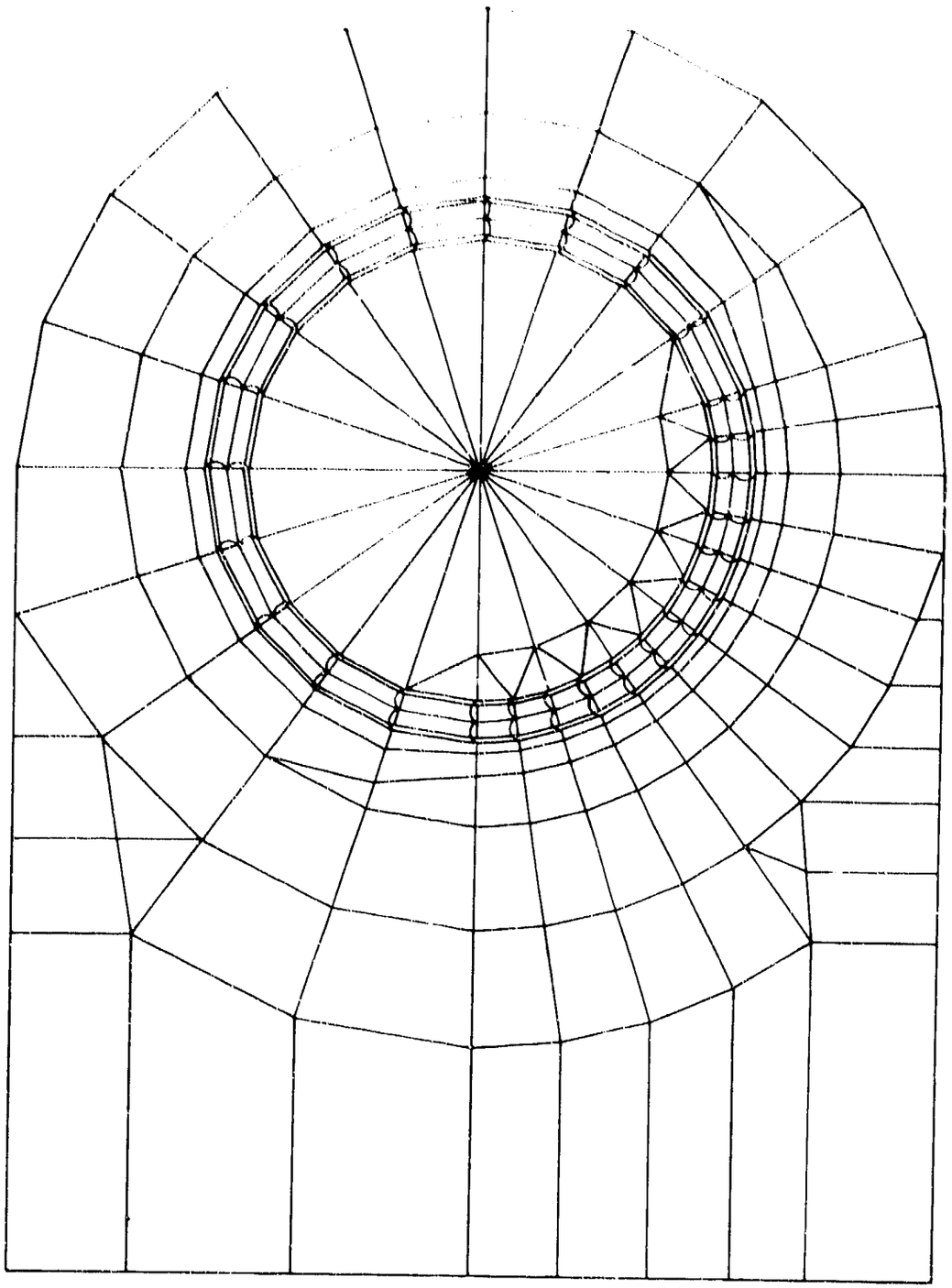

Figure 26. Idealized Lug for Finite-Element Analysis.

Concentration Factor for Tangential Stress

Figures 27 and 28 present values for K_{br} to be used for lug analysis, and Figure 29 shows the angular position at which the maximum stress occurs. The data shown in these figures correspond to the idealized lug conditions that are shown and described in Figure 10, Case 3, wherein only radial compressive stress is assumed to exist between the lug and the liner. Figures 27, 28, and 29 constitute a concise summary and an extension of the results of the finite-element analyses. The data points shown in these figures correspond to the specific geometries for which calculations were made. The curves can be used for either steel or titanium lugs.

During the course of the work, additional information of general background interest concerning the state of stress in lugs was developed which never found direct application in the method adopted herein for predicting the fatigue strength. Some of this information is presented in Figure 30 and Table VI. Figure 30 provides a more detailed look at the state of stress around the entire periphery of the bore of a lug for several orientations of load. The lug had the dimensions of a test lug with W/D = 1.7; the load was 1 kip. Table VI summarizes the values of K_{br} and θ_s that were obtained from the finite-element analyses. It is noted that data are included for the behavior of lugs with idealized behavior corresponding to Cases 1, 2, and 3 shown in Figure 10. The data for Case 3 were used to prepare Figures 27 through 29.

Tangential Stress From Interference Fit

The tangential stress f_i in the lug caused by the interference fit between the lug and the liner can be calculated by multiplying the Lamé solution for thick-walled cylinders (with diameters d, D, and W, and interference i) by an appropriate modification factor K_i determined from Figure 31. The value of K_i should be selected at θ_s, the angle at which the maximum stress from mechanical loading occurs.

The modification factors were obtained from finite-element analyses of a steel lug with a steel liner that had D/d = 1.184. In the analysis it was assumed that friction prevented relative tangential slippage between the liner and the lug. Additional analyses using a titanium lug and a steel liner produced essentially the same results; therefore, Figure 31 can be used for either steel or titanium lugs.

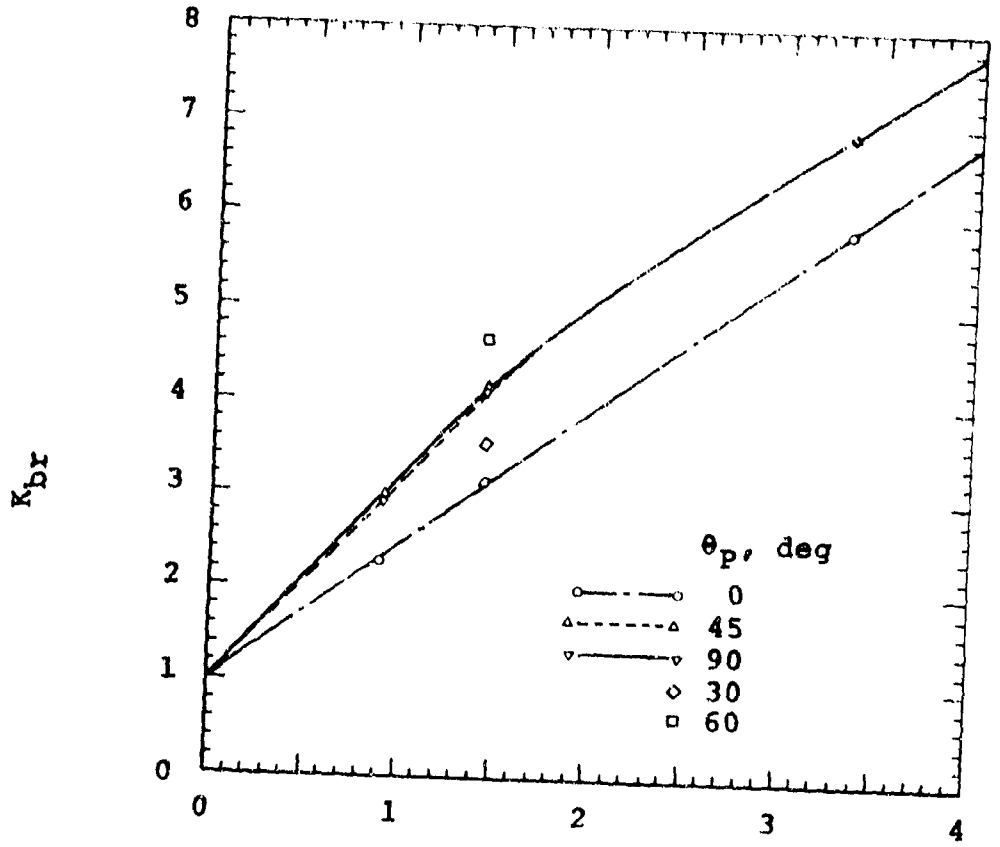

Figure 27. Stress Concentration Factor K_{br} Versus Ratio of Diameter to Net Section.

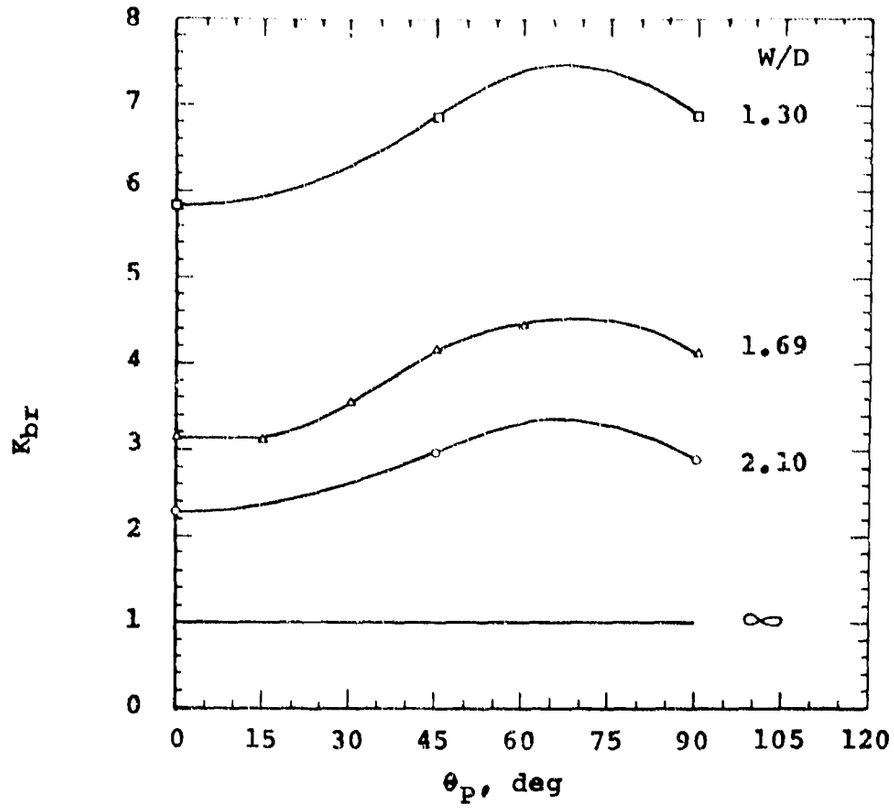

Figure 28. Stress Concentration Factor Kbr Versus Angle of Load.

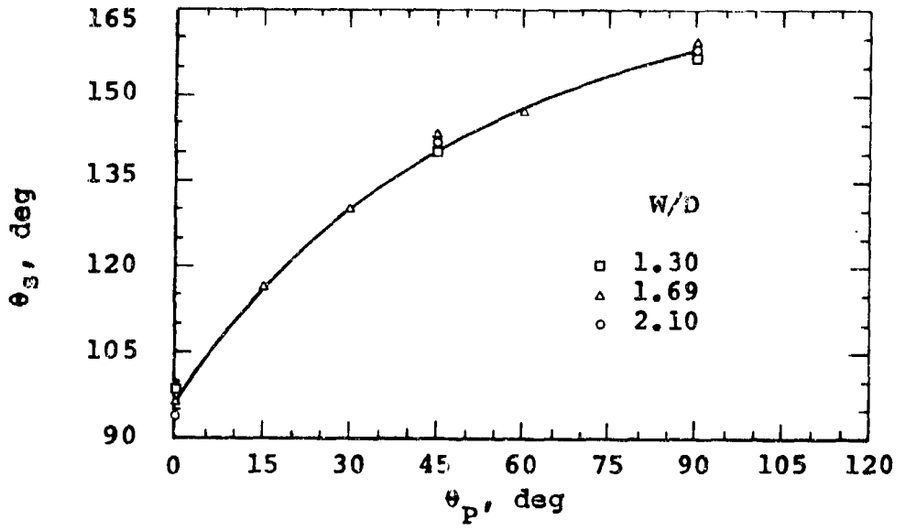

Figure 29. Angular Position of Maximum Tangential Stress Versus Angle of Load.

TABLE VI. SUMMARY OF K_{br} AND θ_s FROM FINITE-ELEMENT ANALYSES

W/D	θ_p deg	K_{br} for Cases *			θ_s for Cases		
		1	2	3	1	2	3
1.30	0	2.55	4.20	5.86	91.	100.	98.
	45	3.08	5.51	6.90	138.	144.	140.
	90	3.26	5.56	6.90	148.	157.	155.
1.69	0	1.81	2.74	3.14	92.	99.	96.
	15			3.11			116.
	30			3.55			131.
	45	2.25	3.61	4.17	138.	144.	142.
	60			4.45			147.
	90	2.34	3.58	4.14	148.	156.	159.
2.10	0		2.01	2.28		98.	94.
	45		2.62	2.99		143.	142.
	90		2.60	2.91		157.	158.

* The cases are described in Figure 10.

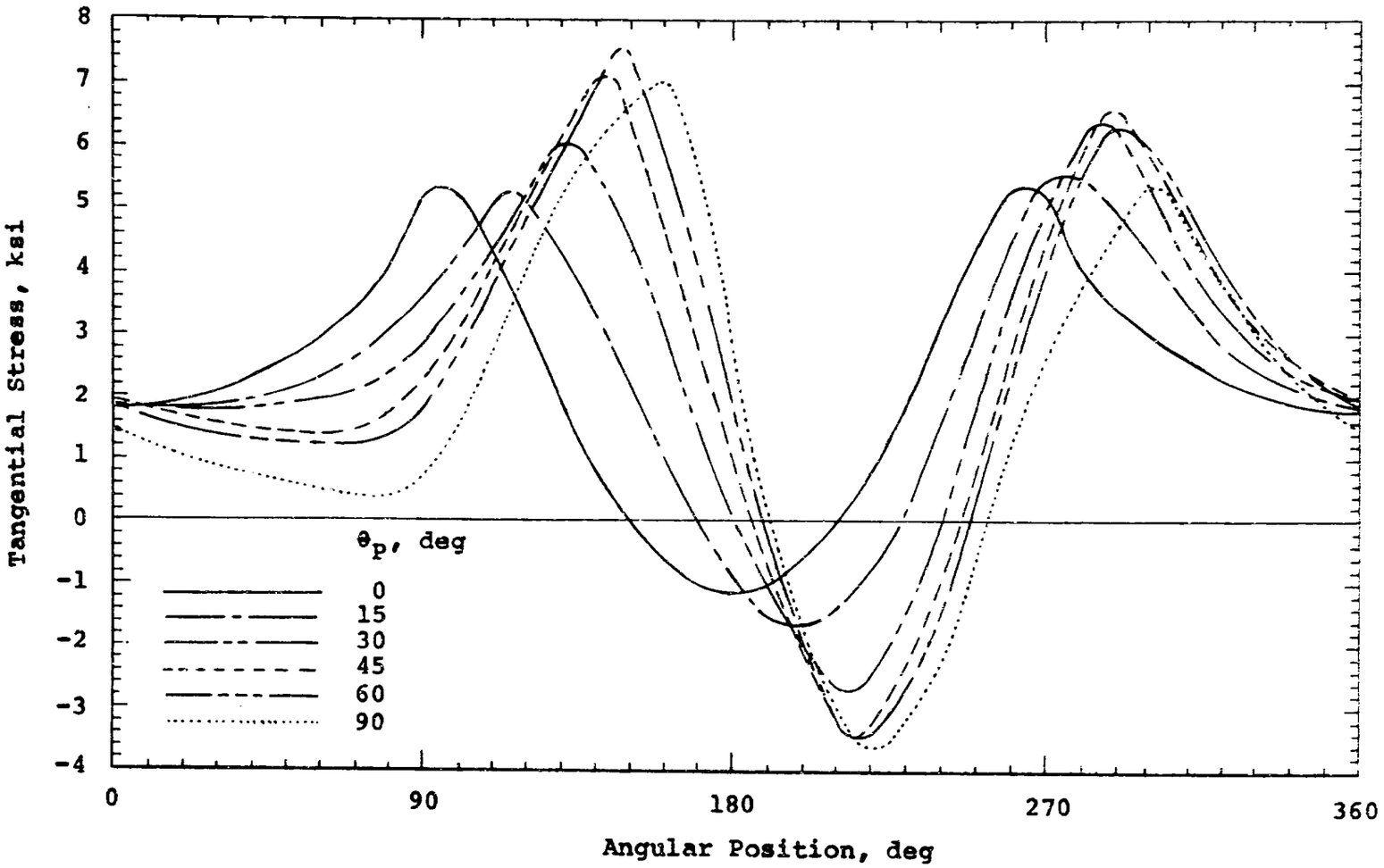

Figure 30. Tangential Stress Versus Angular Position.

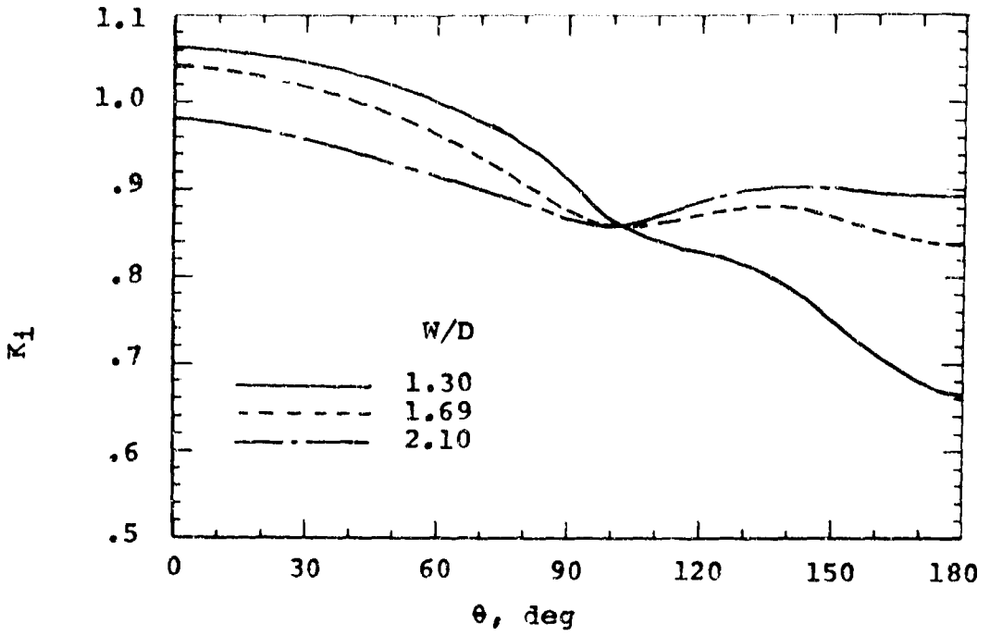

Figure 31. Tangential Stress Factor K_i Versus Angular Position

Bearing Stress for Gap

The bearing stress f_g can be calculated by dividing the Lame solution for radial pressure between two thick-walled cylinders (with diameters d, D, and W, and interference i) by a factor K_r determined from Figures 32 and 33.

These factors were found from finite-element analyses, which assumed that only radial forces existed between the liner and the lug around the entire bore. These analyses used D/d = 1.184. The factor K_r has a physical interpretation. It is the average radial tension stress that existed in the idealized links over a 90-degree arc of the bore in a position approximately opposite to the direction of loading for a loading at the pin corresponding to P/DT = 1.0.

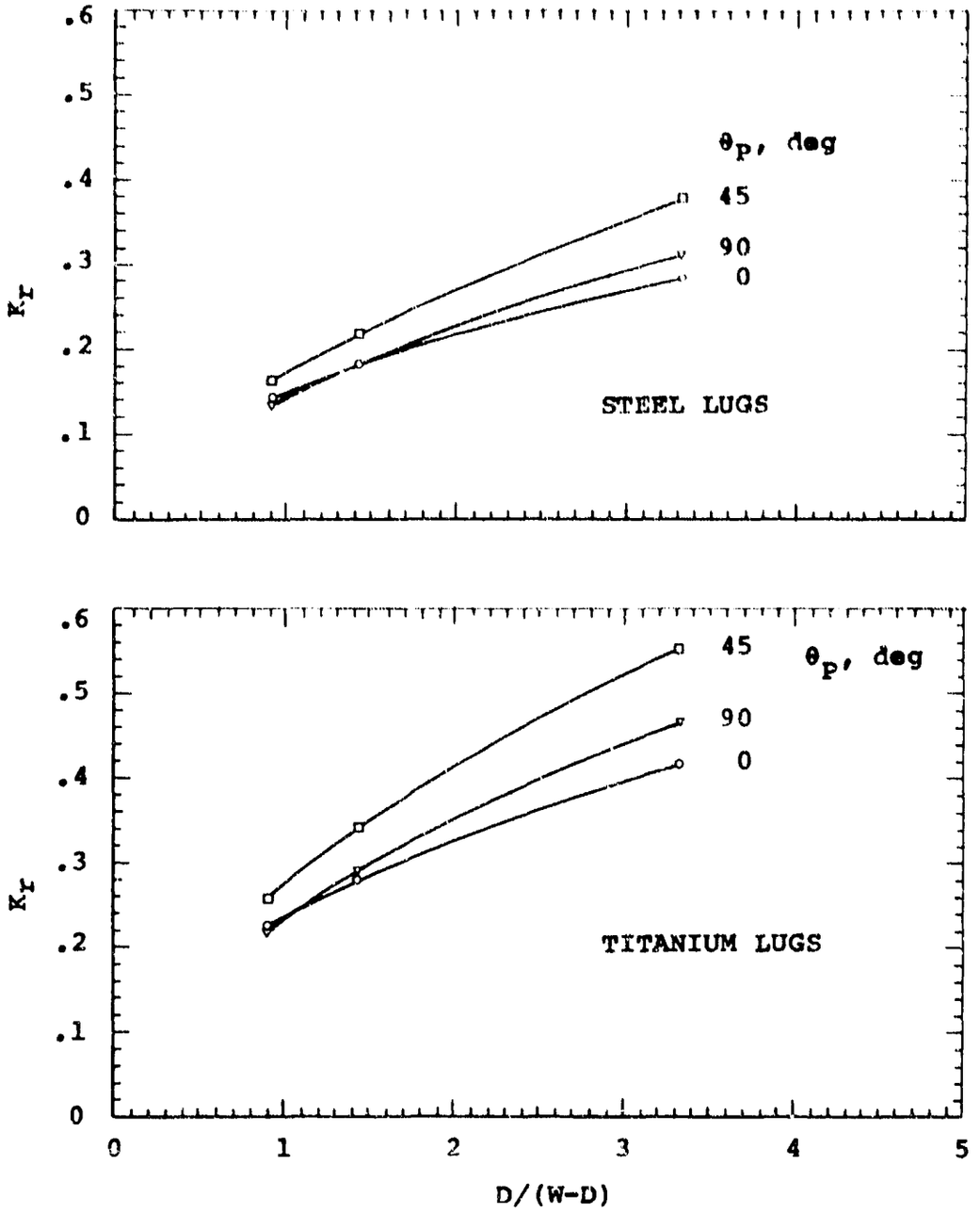

Figure 32. Radial Stress Factor K_r Versus Ratio of Diameter to Net Section.

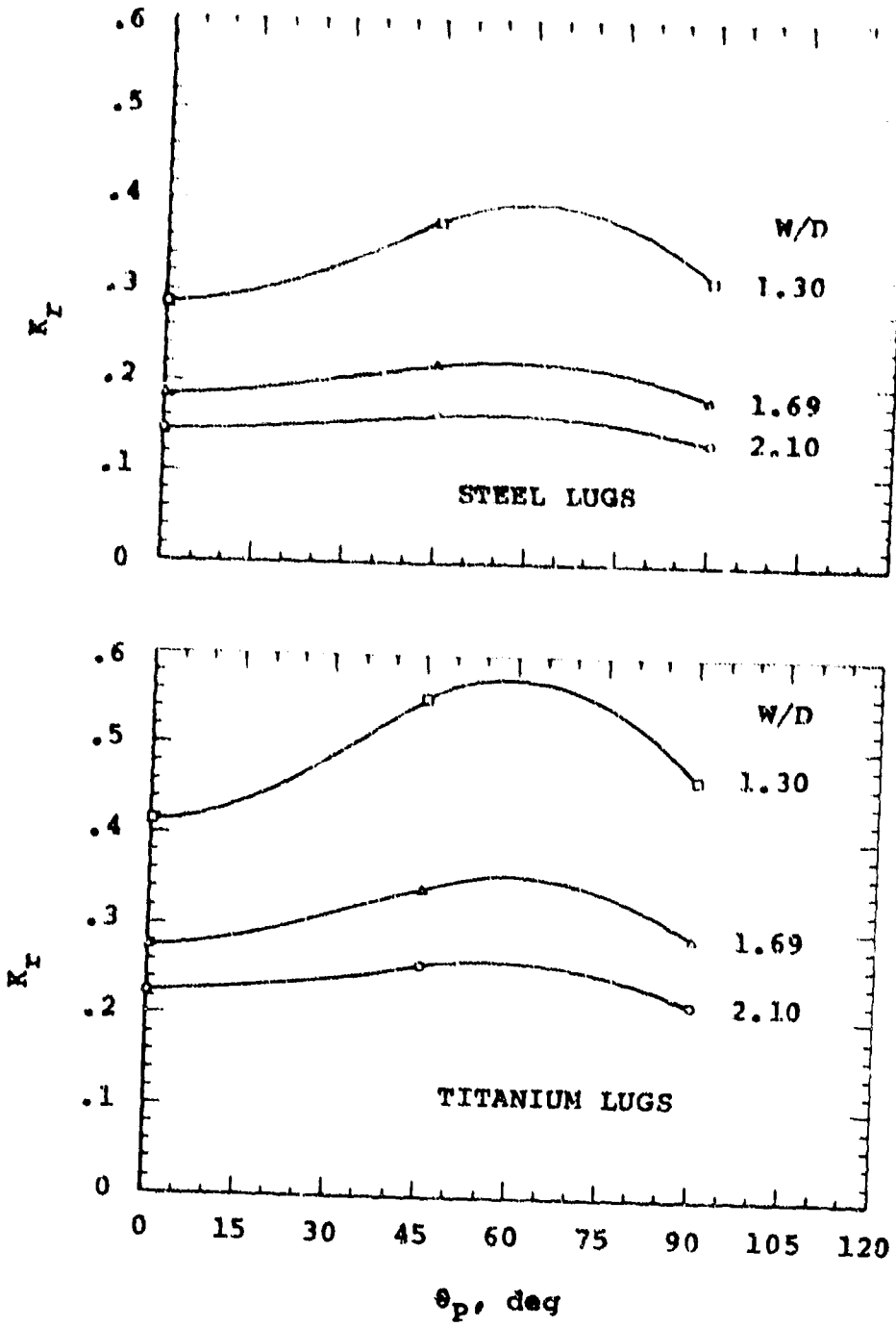

Figure 33. Radial Stress Factor K_r Versus Load Angle.

EXAMPLE

This example shows the construction and use of a stress-versus-load relationship and a design curve.

Given:

A steel lug with a steel liner is loaded by a mean load P_{mean} and a superimposed alternating load P_{alt}.

E = 29,000 ksi
d = 1.000 in.
D = 1.184
T = .500 in.
W = 2.000 in.
i/D = .001
θ_p = 45°

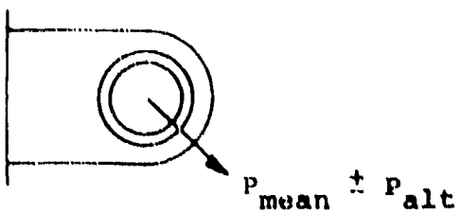

It is desired that the life exceed 10^7 cycles with p = .10 and γ = .90.

Required:

(1) stress-versus-load relationship
(2) design curve
(3) allowable alternating load if the mean load = 12 kips

Solution for (1):

The stress-versus-load relationship constructed here is applicable to any steel lug with a steel liner having the same E, d/D, i/D, and θ_p.

W/D = 1.69
D/(W-D) = 1.184/.816 = 1.45
K_{br} = 4.17 from Figure 27 or 28, Table VI
θ_s = 142° from Figure 29, or Table VI
K_i = .881 from Figure 31
K_r = .219 from Figure 32 or 33

The calculations for f_g and f_i involve the Lamé solution for an interference fit of two concentric cylinders with diameters d, D, and W. The Lamé solution can be found in reference 11.

f_g = Lamé radial stress between the cylinders/K_r
f_i = K_i x Lamé tangetial stress at the bore of the outer cylinder

f_g = 4.784/.291 = 16.44 ksi
f_i = (.881) (7.480) = 6.59 ksi

C_1 = 1.3
C_2 = .8 - $(180-\theta_p)(7\ i/D)^2$ = .793
C_3 = 2.6

$C_1 f_g$ = 21.37 ksi
$C_1 C_2 K_{br} f_g$ = 70.67 ksi
$C_3 f_g$ = 42.74 ksi
$C_3 f_g K_{br}$ = 178.24 ksi

The required relationship is:

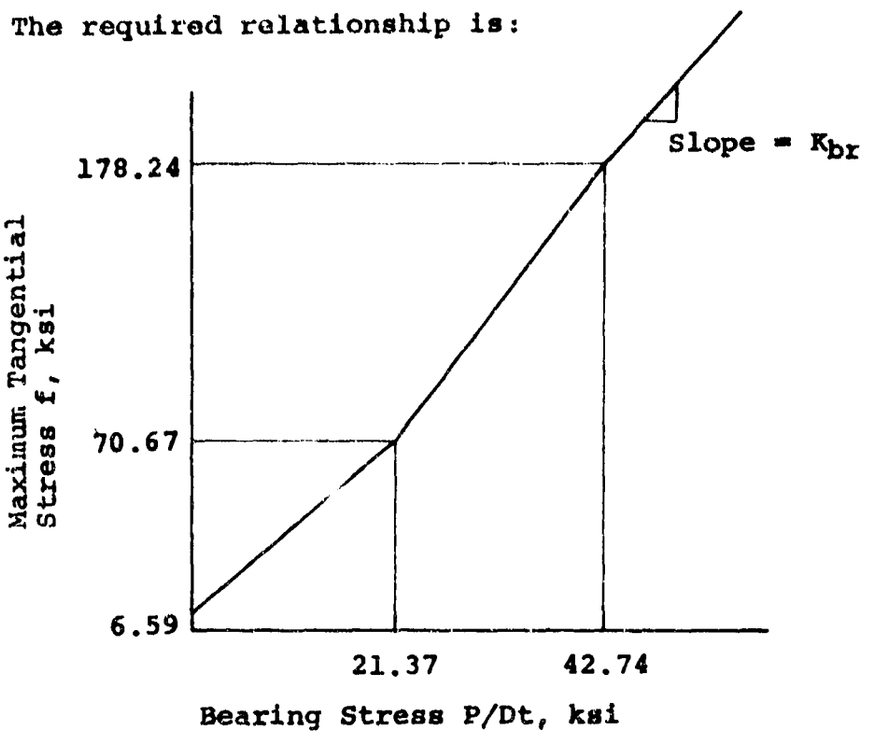

Solution for (2):

The design curve was constructed using:
a) the stress-versus-load relationship from solution (1),

b) an allowable alternating stress F_a = 18.7 ksi from Table V,

c) the maximum stress f_{max} = 115 ksi experienced during tests shown in Figure 13, and

d) an ultimate static strength/DT = 99.45 ksi calculated from Melcon and Hoblit, reference 2.

The required design curve is:

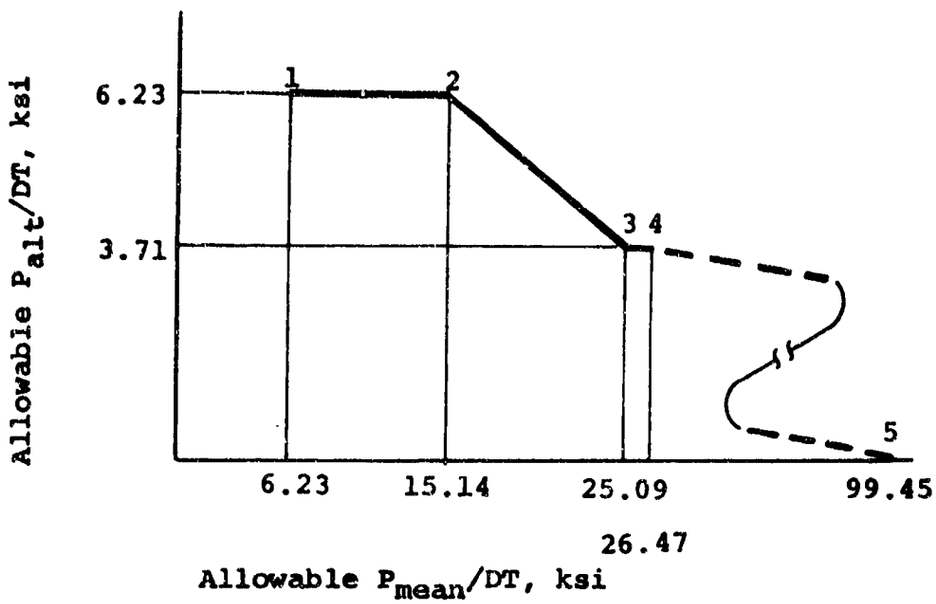

The straight-line segments of the design curve are a natural consequence of the stress-versus-load relationship and an F_a which is independent of mean stress. Slight fairings of the lines at the junctions would be appropriate; however, they are omitted here for clarity in description of the curve.

Points 1, 2, and 3 correspond to changes in direction of the stress-versus-load curve. Point 4 corresponds to f_{max} = 115 ksi and F_a = 18.7 ksi. Point 5 is the ultimate static strength calculated from Melcon and Hoblit using a material ultimate strength = 175 ksi. The solid-line portion of the curve corresponds to a maximum stress less than 115 ksi and thus is within the experience of the fatigue tests. The

dotted-line portion of the curve corresponds to loads that cause f_{max} to be greater than 115 ksi and thus represents extrapolated performance.

The data for the points are shown below:

Stress		Point 1	2	3	4	5
f_{min}	ksi	6.59	33.27	70.67	77.60	--
f_{max}*	ksi	43.99	70.67	108.07	115.00	--
P_{min}/DT	ksi	0	8.90	21.37	22.75	--
P_{max}/DT	ksi	12.47	21.37	28.80	30.18	--
P_{mean}/DT	ksi	6.23	15.14	25.09	26.47	99.45
P_{alt}/DT	ksi	6.23	6.23	3.71	3.71	0

* $f_{max} = f_{min} + 2F_a$

Solution for (3):

$P_{mean}/DT = 20.27$ ksi

Using the design curve,

$$P_{alt}/DT = 3.71 + \frac{(25.09 - 20.27)}{(25.09 - 15.14)} (6.23-3.71) = 4.93 \text{ ksi}$$

$P_{alt} = 4.93DT = \underline{\underline{2.92 \text{ kips}}}$.

This result can be checked using the stress-versus-load relationship. The alternating tangential stress should be 18.7 ksi for P = 12.0 ±2.92 kips.

$P_{min}/DT = (12. - 2.92)/.592 = 15.34$ ksi

$P_{max}/DT = (12. + 2.92)/.592 = 25.20$ ksi

$$f_{min} = 6.59 + \frac{(15.34)}{21.37}(70.67 - 6.59) = 52.59 \text{ ksi}$$

$$f_{max} = 70.67 + \frac{(25.20 - 21.37)}{(42.74 - 21.37)}(178.24 - 70.67) = 89.95 \text{ ksi}$$

$f_{alt} = .5\ (f_{max} - f_{min}) = 18.7$ ksi, check

CONCLUSIONS

1. The vibrating beam apparatus performed well and was a practical and economical means for fatigue testing.

2. Reliable data were obtained for the long-endurance fatigue strength of lugs containing interference-fitted liners. The tests covered a significant range of lug geometries, load orientations, and interference fits.

3. A rational analysis was developed for the long-endurance fatigue strength of lugs containing interference-fitted liners. The analysis showed good correlation with test results.

4. The finite-element method was a practical and flexible tool for determining the elastic stresses in detail.

5. Allowable stresses were determined for high-quality steel and titanium lugs for several probabilities of failure.

6. Simple procedures were developed for the direct design for long endurance of steel and titanium lugs containing interference-fitted liners.

7. High interference between the liner and the lug significantly improves the fatigue performance and reliability for long-endurance applications. The greatest benefit of interference is produced in steel lugs designed for low probability of failure. For such lugs high interference can nearly double the allowable alternating load.

8. Direct comparisons of allowable loads for steel and titanium lugs can be made from the design charts. In general, a steel lug is roughly 25 percent stronger than a titanium lug of identical dimensions. An outstanding exception to this generalization occurs in the case of a lug with low interference fit designed for high reliability. For such lugs the titanium and steel lugs have roughly equal allowable alternating loads for moderately low load ratio R.

RECOMMENDATION

It is recommended that many important areas that were beyond the scope of the present effort be considered for inclusion in future programs for structural research. These areas include the investigation of lug performance for additional loading conditions, geometries, and materials. Additional loading conditions of prime practical importance for helicopter applications are: high load ratio, high vibratory load, and spectrum loading. The effort for high load ratio would investigate the dashed-line regions on the design curves reported herein. The work on high vibratory load would be concerned with conditions that cause failure in less than 10^7 cycles. The spectrum loading investigations would determine the applicability of cumulative damage concepts for high vibratory loads. Additional geometrical investigations would determine the optimum proportions for the liner relative to the lug, the performance of lugs with non-parallel sides, and the performance of lugs with variable thickness. Investigations of additional materials should include aluminum alloys, maraging steels, and filamentary reinforced composites.

LITERATURE CITED

1. A GUIDE FOR FATIGUE TESTING AND THE STATISTICAL ANALYSIS OF FATIGUE DATA, American Society for Testing Materials, STP-91A, 1963.

2. Melcon, M.A., and F. M. Hoblit, DEVELOPMENTS IN THE ANALYSIS OF LUGS AND SHEAR PINS, Product Engineering, June 1953.

3. METALLIC MATERIALS AND ELEMENTS FOR FLIGHT VEHICLE STRUCTURES, MIL-HDBK-5, March 1961; Revised June 1, 1965.

4. Frocht, M.M., PHOTOELASTICITY, VOL. II., John Wiley and Sons, 1948, pp. 179-193.

5. Heywood, R.B., THE STRENGTH OF LUGS IN FATIGUE, Royal Aircraft Establishment Technical Note No: Structures 182, January 1956.

6. Grover, H.J., FATIGUE OF AIRCRAFT STRUCTURES, Naval Air Systems Command, Department of the Navy, NAVAIR 01-1A-13, 1966.

7. Dixon, J.R., and H. M. Scott, EFFECT OF NON-AXIAL LOADING ON STRESS DISTRIBUTION IN PLATES LOADED THROUGH PIN JOINTS, NEL Report No. 108, National Engineering Laboratory, August 1963.

8. Melts, Richo, PHOTOELASTIC STUDY OF STRESS CONCENTRATIONS OF SINGLE PIN LOADED LUGS IN TENSION, Thesis for M.S. in Civil Engineering, Polytechnic Institute of Brooklyn, June 1964.

9. Lambert, T.H., and R. J. Brailey, THE INFLUENCE OF THE COEFFICIENT OF FRICTION ON THE ELASTIC STRESS CONCENTRATION FACTOR FOR A PIN-JOINTED CONNECTION, The Aeronautical Quarterly, February 1962.

10. Ligenza, S.J., CYCLIC-STRESS REDUCTION WITHIN PIN-LOADED LUGS RESULTING FROM OPTIMUM INTERFERENCE FITS, Experimental Mechanics, January 1963.

11. Seeley, F.B., and J. O. Smith, ADVANCED MECHANICS OF MATERIALS, John Wiley and Sons, 1952.

APPENDIX

COMMENTS ON K_t AND K_{br} FOR AXIALLY LOAD LUGS

This Appendix:

1. presents a relationship between K_t and K_{br},
2. uses the relationship to provide a useful boundary for possible values of K_t, and
3. discusses approximate solutions for K_t and K_{br}.

Relationship Between K_t and K_{br} for $\theta_p = 0$.

By definition,

$$\text{maximum tangential stress} = K_{br} \frac{P}{DT}$$

$$K_t = \frac{\text{maximum tangential stress}}{\text{average stress on net section}}$$

then, $$K_t = K_{br} \frac{P}{DT} \frac{(W-D)T}{P}$$

$$K_t = K_{br} \frac{(W-D)}{D} \qquad (1)$$

Equation 1 is the required relationship. This equation shows also that the parameter (W-D)/D is a natural abscissa for plots of K_t because the curve will approach a straight line as K_{br} approaches a constant value at large W/D. Similarly, D/(W-D) is a natural abscissa for a plot of K_{br}, as shown by Figure 27.

Boundary for K_t with $\theta_p = 0$.

Frocht in reference 4 shows that K_{br} is always greater than 1.0 and approaches 1.0 as a limit at D/W = 0. If we substitute $K_{br} = 1.0$ into Equation 1, we get the desired boundary for K_t, thus:

$$K_t \geq \frac{W-D}{D}$$

$$K_t \geq \frac{W}{D} - 1 \qquad (2)$$

This boundary can be plotted onto conventional plots for K_t such as that shown in Figure 25. The boundary is a useful guide for extrapolating curves or for checking on the extrapolations of others. According to the reasoning presented here, no curve for an axially loaded lug without interference between the pin and the lug can lie below Equation 2.

Approximate Solutions for $\theta_p = 0$.

Page 192 in reference 2 contains a very interesting footnote which states:

"It will be found that as first approximation, for closely fitting pins and H/W greater than unity, the maximum tension equals the sum of the average bearing stress plus 1.5 times the nominal tension."

Thus,

$$f_{max} = f_{\substack{average \\ bearing}} + 1.5\, f_{\substack{average \\ tension}}$$

$$f_{max} = \frac{P}{DT} + 1.5\,\frac{P}{(W-D)T}$$

$$f_{max} = \frac{P}{DT}\left[1 + 1.5\left(\frac{D}{W-D}\right)\right]$$

$$K_{br} = \frac{f_{max}\ DT}{P}$$

$$K_{br} = 1 + 1.5\left(\frac{D}{W-D}\right) \tag{3}$$

Combining Equations 1 and 3, we get

$$K_t = \left(\frac{W-D}{D}\right) + 1.5 \tag{4a}$$

$$K_t = \frac{W}{D} + .5 \tag{4b}$$

Equations 3 and 4 are the required approximate solutions.

It is noted that according to Equation 3, K_{br} should be a straight line with a slope of 1.5 when plotted against the parameter D/(W-D). This is quite consistent with the plot shown in Figure 27.

If Equation 4b is plotted onto Figure 25, it will be seen that Equation 4b is an excellent mean fit to the curves.

Unclassified

Security Classification

DOCUMENT CONTROL DATA - R & D

(Security classification of title, body of abstract and indexing annotation must be entered when the overall report is classified)

1 ORIGINATING ACTIVITY (Corporate author) KAMAN AEROSPACE CORPORATION Old Windsor Road Bloomfield, Connecticut 06002	2a REPORT SECURITY CLASSIFICATION Unclassified 2b GROUP

3 REPORT TITLE

FATIGUE STRENGTH OF LUGS CONTAINING LINERS
VOLUME I RESULTS

4 DESCRIPTIVE NOTES (Type of report and inclusive dates)
Final Report

5 AUTHOR(S) (First name, middle initial, last name)
Robert J. Mayerjak
Paul F. Maloney

6 REPORT DATE	7a TOTAL NO OF PAGES	7b NO OF REFS
November 1970	93	11

8a CONTRACT OR GRANT NO	9a ORIGINATOR'S REPORT NUMBER(S)
DAAJ02-67-C-0066 N/ W/ b PROJECT NO Task 1F162204A14601 c d	USAAVLABS Technical Report 70-49A 9b OTHER REPORT NO(S) (Any other numbers that may be assigned this report) KAC Report No. R-850, Volume I

10 DISTRIBUTION STATEMENT
This document is subject to special export controls, and each transmittal to foreign governments or foreign nationals may be made only with prior approval of U. S. Army Aviation Materiel Laboratories, Fort Eustis, Virginia 23604.

11 SUPPLEMENTARY NOTES	12 SPONSORING MILITARY ACTIVITY
	U.S. Army Aviation Materiel Laboratories Fort Eustis, Virginia

13 ABSTRACT

This report presents the results of an investigation of the fatigue strength of structural lugs. The program included both experimental and analytical phases which were used in a complementary fashion to formulate design charts for fatigue-loaded steel and titanium lugs containing interference-fit liners. These lugs are representative of design practice in highly loaded aircraft applications, particularly that found in helicopter blade attaching systems. A primary element in the analytical study was a two-dimensional structural analysis of lug configurations, which was done by finite element methods using a computer program. This computer program is published in Volume II of this report.

The design charts presented will permit the designer to rapidly select lug proportions in either steel or titanium that will satisfy structural requirements for a range of steady and vibratory loading. The designs are considered to be particularly applicable to helicopter rotor and control systems.

DD FORM 1 NOV 68 1473 REPLACES DD FORM 1473, 1 JAN 64, WHICH IS OBSOLETE FOR ARMY USE.

Unclassified
Security Classification

14 KEY WORDS	LINK A		LINK B		LINK C	
	ROLE	WT	ROLE	WT	ROLE	WT
Fatigue St ngth of Steel and Titanium Structural Lugs						
Two-dimensional Structural Analysis						
Aircraft Design						
Finite Element Computer Program						